



HAL
open science

**The mafic-silicic layered intrusions of
Saint-Jean-du-Doigt (France) and North-Guernsey
(Channel Islands), Armorican Massif: Gabbro-diorite
layering and mafic cumulate-pegmatoid association**

Martial Caroff, Nolwenn Coint, Erwan Hallot, Cédric Hamelin, Jean-Jacque
Peucat, Gilles Charretour

► **To cite this version:**

Martial Caroff, Nolwenn Coint, Erwan Hallot, Cédric Hamelin, Jean-Jacque Peucat, et al.. The mafic-silicic layered intrusions of Saint-Jean-du-Doigt (France) and North-Guernsey (Channel Islands), Armorican Massif: Gabbro-diorite layering and mafic cumulate-pegmatoid association. *Lithos*, 2011, 125, pp.675-692. 10.1016/j.lithos.2011.03.019 . insu-00589245

HAL Id: insu-00589245

<https://insu.hal.science/insu-00589245>

Submitted on 28 Apr 2011

HAL is a multi-disciplinary open access archive for the deposit and dissemination of scientific research documents, whether they are published or not. The documents may come from teaching and research institutions in France or abroad, or from public or private research centers.

L'archive ouverte pluridisciplinaire **HAL**, est destinée au dépôt et à la diffusion de documents scientifiques de niveau recherche, publiés ou non, émanant des établissements d'enseignement et de recherche français ou étrangers, des laboratoires publics ou privés.

1 The mafic-silicic layered intrusions of Saint-Jean-du-Doigt
2 (France) and North-Guernsey (Channel Islands), Armorican
3 Massif: gabbro-diorite layering and mafic cumulate-pegmatoid
4 association

5
6 Martial Caroff^{a,*}, Nolwenn Coint^{a,1}, Erwan Hallot^b, Cédric Hamelin^{a,2}, Jean-Jacques Peucat
7 ^b, Gilles Charreteur^b
8

9 ^aUMR CNRS 6538 « Domaines Océaniques », IUEM, Université de Brest, 6 avenue Victor
10 Le Gorgeu, CS 93837, 29238 Brest cedex 3, France

11 ^b Géosciences Rennes, UMR CNRS 6118, Université de Rennes 1, 35042 Rennes cedex,
12 France
13

14 * Corresponding author: caroff@univ-brest.fr
15

16 ¹ Present address : Department of Geosciences, Texas Tech University, Lubbock, TX 79409,
17 USA (nolwenn.coint@ttu.edu)

18 ² Present address : IPGP, Laboratoire de Géosciences Marines, 4, Place Jussieu 75252 Paris
19 cedex 05, France

20 Abstract

21

22 The Saint-Jean-du-Doigt (France) and North-Guernsey (Channel Islands) Intrusive
23 Complexes (hereafter referred to as SJIC and NGIC, respectively) are examples of mafic-
24 silicic layered intrusions in the Armorican Massif. Both are characterized by the occurrence of
25 (1) a basal/peripheral gabbroic unit interlayered with sheets (generally dioritic in composition,
26 occasionally gabbroic) and crossed by leucocratic diapirs and pipes (from monzodioritic to Q-
27 monzonitic in composition), (2) peripheral pegmatoids associated with mafic cumulates and
28 (3) coeval granitoids. Beside these main similarities, some contrasted features lead us to
29 propose two distinct models of formation. The Variscan SJIC includes tholeiitic mafic rocks
30 (monzogabbro) that locally mingle and mix with leucocratic components (monzonite or Q-
31 monzonite). The Cadomian NGIC is calc-alkaline. The SJIC sheet-bearing gabbro is
32 homogeneous from a petrologic point of view, whereas the NGIC exhibits gabbroic
33 macrorhythmic sequences with mineral layering. The Sr-Nd isotopic compositions of the SJIC
34 gabbros are significantly different from those of the associated dioritic layers. This is not the
35 case in the NGIC where the magmas could be cogenetic. We argue that the SJIC gabbro was a
36 liquid that crystallized *in situ* without significant crystal settling. By contrast, the rhythmic
37 sequences of the NGIC are consistent with crystal accumulation. Subsequently, both can be
38 seen as mafic reservoirs which were repeatedly invaded by magmas of intermediate
39 composition. We interpret the sheets in the SJIC as the result of horizontal spreading of
40 dioritic metastable magmas into a gabbroic reservoir crystallizing from below, at levels of
41 neutral buoyancy. Injections and convection in the central part of the reservoir possibly
42 resulted in spectacular mixing/mingling structures. In the NGIC, the emplacement of the
43 dioritic sheets was rather controlled by pre-existing rhythmic cumulative structures. In both
44 intrusions, late differentiated diapirs were extracted from the dioritic sheets. Associated

45 peripheral pegmatoids are thought to result from the crystallization of liquids issued from a
46 mafic intercumulus melt in the presence of a fluid phase. This extraction might have been
47 enhanced by the disruption of the peripheral cumulate stack, perhaps following pressure
48 drops.

49

50 *Keywords:* Gabbro; Diorite; Granite; Layered intrusion; Replenishment; Armorican Massif

51

52 **1. Introduction**

53

54 The term MASLI (MAfic-Silicic Layered Intrusion), as first proposed by Wiebe
55 (1993a and b), refers to plutonic complexes with interlayered mafic (gabbroic) and
56 intermediate/felsic (dioritic to granitic) rocks (Wiebe, 1996; Franceschelli et al., 2005).

57 MASLIs can be recognized by distinctive field relationships which always include (i) lobate
58 contacts between the main gabbro-dioritic intrusions and surrounding or underlying
59 granitic/granodioritic plutons and (ii) layers, sheets, diapirs, and/or veins of dioritic/silicic
60 material into gabbroic units (Wiebe, 1996). Other features commonly (but not always)
61 described in such complexes are: (iii) macrorhythmic gabbro-dioritic units, from less than one
62 to several tens of meters thick, with chilled bases (Wiebe, 1993b, 1994, 1996; Waight et al.,
63 2007), (iv) modal layering and feldspar lamination in the dioritic/silicic layers (Wiebe, 1996),
64 (v) mafic/intermediate enclaves in the granites (Wiebe, 1994; Wiebe et al., 1997), and (vi)
65 basaltic pillow-like chilled bodies within felsic units (Wiebe, 1974, 1993b; Wiebe et al.,
66 2001). Although differences exist between the examples, Wiebe and others first proposed a
67 comprehensive model to account for these features: repeated mafic injections into a felsic
68 chamber, from dioritic to granitic composition, followed by fractional crystallization and
69 complex liquid-liquid (and/or partially crystallized magma-magma) interactions including

70 small scale diapirism and hybridization. More recently, MASLIs were recognized to result
71 from multiple replenishments of mafic and felsic magmas, mingling and limited mixing, and
72 rejuvenation of granite (Wiebe et al., 2007).

73 If the Cadomian layered gabbro-diorite complex of North-Guernsey (Channel Islands)
74 was suspected by Wiebe (1996) to be a MASLI, the Variscan intrusion of Saint-Jean-du-Doigt
75 (France) was never considered as such. However, both Armorican plutonic bodies display
76 many of the features characteristic of mafic-silicic layered intrusions. Additionally, both
77 complexes show spectacular pegmatoid (gabbroic pegmatite) occurrences systematically
78 associated with coarse-grained mafic cumulates. Such a lithologic association has already
79 been described in various gabbroic intrusions (Smartville intrusive complex, California:
80 Beard and Day, 1986; Kraemer macrodyke, Greenland: Momme and Wilson, 2002; Mount
81 Sheridan gabbro, Oklahoma: McEllen, 2006), but not specifically in MASLIs. In spite of their
82 similarities, each Armorican intrusion shows distinctive petrological and geochemical
83 (isotopic) characters.

84 The aim of this study is to reexamine the published models of MASLI formation
85 through these two new examples from the Armorican Massif, which display both shared and
86 contrasted features. This leads us to propose distinct processes of construction emphasizing
87 the possibility that replenishment of mafic chambers by intermediate partially crystallized
88 magmas explains some features of MASLIs.

89

90 **2. Analytical techniques**

91

92 Compositions of mineral phases were obtained with a Cameca SX50 automated
93 electron microprobe (Microsonde Ouest, Brest). Analytical conditions were 15 kV, 15 nA,

94 counting time 6 s, correction by the ZAF method. Concentrations <0.3% are considered
95 qualitative.

96 Major and trace element compositions (Table 1) were measured at the University of
97 Brest on whole rock powders by inductively coupled plasma atomic emission spectrometry
98 (ICP-AES). Analytical methods are described in Cotten et al. (1995). Relative standard
99 deviations are <2% for major elements and <5% for trace elements. For the coarsest-grained
100 samples, a large quantity of rock was crushed in a steel jaw-crusher (e.g., 20 kg for the
101 pegmatoid SJ16). After the crushed rock was quartered, a representative split was pulverized
102 in an agate mill.

103 The Sr-Nd isotopic compositions were obtained from whole rock powders with a
104 Cameca TSN 206 mass spectrometer (Guernsey) and with a Finnigan MAT 262 mass
105 spectrometer (Saint-Jean-du Doigt) at Géosciences Rennes. Sr, Rb, Sm and Nd contents were
106 measured by isotope dilution except for the SJIC samples in which Rb was determined by
107 ICP-AES. Errors on $^{87}\text{Rb}/^{86}\text{Sr}$ and $^{147}\text{Sm}/^{144}\text{Nd}$ ratios are 2% and 1%, respectively. Details of
108 analytical procedures are described in Peucat et al. (1999). $^{87}\text{Sr}/^{86}\text{Sr}$ ratios were normalized to
109 the NBS 987 standard ($^{87}\text{Sr}/^{86}\text{Sr} = 0.71025$) and $^{143}\text{Nd}/^{144}\text{Nd}$ ratios to the AMES standard
110 ($^{143}\text{Nd}/^{144}\text{Nd} = 0.511963$). ϵ_{Nd} values, in Table 2, were calculated using $^{143}\text{Nd}/^{144}\text{Nd}_{\text{CHUR}} =$
111 0.51264 and $^{147}\text{Sm}/^{144}\text{Nd}_{\text{CHUR}} = 0.1967$. They correspond to: $\epsilon_{(t)} = 10^4((^{143}\text{Nd}/^{144}\text{Nd}_{\text{sample}} /$
112 $0.51264) - 1)$ and $\epsilon_{(t)} = \epsilon_{(0)} - (25.1((^{147}\text{Sm}/^{144}\text{Nd}_{\text{sample}} - 1) / 0.1967)\Delta_{(t)})$, following De Paolo
113 (1988).

114

115 **3. Saint-Jean-du-Doigt Intrusive Complex (SJIC)**

116

117 *3.1. Geology*

118

119 The Saint-Jean-du-Doigt Intrusion (SJIC) is located between the Trégor Cadomian
120 domain, mainly composed of volcanoclastic formations overlying a Palaeoproterozoic
121 (Icartian) gneissic basement (*c.* 2.0 Ga, Auvray et al., 1980), and the Léon Hercynian
122 metamorphic domain (Fig. 1a). The SJIC is composite and includes four main units: the
123 Primel cumulate-pegmatoid association, the Saint-Jean-du-Doigt monzogabbro-(Q-
124)monzonite mingled/mixed rocks, the Poul Rodou layered gabbro-diorites and several granitic
125 bodies (Fig. 1b). Some doleritic dykes cross cut the units, but were not found in the granitic
126 rocks. Most rocks have isotropic textures and exhibit no significant regional deformation
127 subsequent to their emplacement, with the exception of local brittle faulting. However, they
128 have undergone late- to post-magmatic alterations, resulting in the transformation of some
129 primary minerals, without significant change in bulk rock chemistry (Coint et al., 2008). The
130 SJIC was emplaced under a lithostatic pressure of about 0.5 GPa, i.e. at *c.* 15 km depth
131 (amphibole geobarometry: Johnson and Rutherford, 1989 and Schmidt, 1992 *in* Coint et al.,
132 2008), within Proterozoic rocks and Devonian-Carboniferous sediments. Chantraine et al.
133 (1986) have reported a carboniferous U-Pb zircon age of *c.* 350 Ma for the gabbros (Deutsch,
134 unpublished) confirmed by Barboni et al. (2008, 2010), who obtained U-Pb zircon ages at 347
135 \pm 4 Ma for the mafic units and the granitic bodies from Poul Rodou. The SJIC was later
136 intruded by red granites at *c.* 300 Ma (Fig. 1b). The SJIC mafic rocks have a tholeiitic affinity
137 (Chantraine et al., 1986; Coint et al., 2008, 2009; see also section 5.2). Geochemical features
138 of intermediate/felsic rocks are rather typical of calc-alkaline suites (Barboni et al., 2010;
139 Capdevila, 2010).

140

141 *3.2. Coastal SJIC from East to West*

142

143 The Saint-Jean-du-Doigt Intrusive Complex is best exposed along the northern
144 shoreline. Field observations have been made from Poul Rodou to Primel through the bay of
145 Saint-Jean-du-Doigt (Fig. 1b).

146

147 *3.2.1. Poul Rodou: gabbro-diorite layering*

148 From southeast to northwest, the Poul Rodou cross-section begins with a small
149 granitic body in sharp intrusive contact with a Proterozoic formation (Fig. 1b and 2a). The
150 granite is equigranular and intrudes an intergranular/oikocrystic gabbro. Lobate contacts
151 between the granite and the adjacent gabbro and gabbroic enclaves within the granite are
152 interpreted as evidence for the contemporaneous crystallization of both magmas. Other
153 granitic intrusions crop out along the shoreline, such as the Beg ar Fri granite (sample SJ22,
154 Fig 1b and 2a). Several sub-parallel leucocratic sheets form layers within the gabbro. They are
155 oriented SE-NW and dip slightly (10° to 30°) toward the northeast. They are cut
156 southeastward by the granitic intrusion (Fig. 2a). This demonstrates the lack of apparent direct
157 link between leucocratic sheets and granitic bodies. Leucocratic sheets are thin (a few
158 decimeters thick) and sparse near the edge of the complex. They become thicker (up to
159 several decimeters) and more abundant to the northwest. The spacing from one sheet to
160 another varies from several decameters to a few meters. The upper contact with the overlying
161 gabbro is systematically undulated, sometimes connected to felsic masses, a few decimeters in
162 size, within the overlying gabbro (Fig. 3a, b). When elongated, these structures are orientated
163 sub-perpendicularly to the sheet layers. They are interpreted as gravity-driven felsic diapirs
164 extracted from the sheets. In the present orientation, these instabilities are not sub-vertical and
165 the sheets are not sub-horizontal. The variable dipping angles of the structures along the Poul
166 Rodou shoreline are consistent with post-emplacement brittle deformation and denotes
167 northeastward tilting of blocks limited by NE-SW faults (Fig. 2a). The composition of the

168 leucocratic sheets is dioritic, with the exception of their upper part, sometimes Q-monzonitic
169 (Table 1). All are moderately cumulative in plagioclase (cumulus from 20% at the base to
170 50% at the top of the sheets) and generally exhibit an intergranular texture. Felspar-rich
171 (plagioclase and orthoclase) diapirs, more differentiated than their related sheets, have
172 textures ranging from intergranular to pegmatitic. Contrasting with the upper contacts, bases
173 of the leucocratic sheets form relatively regular surfaces with the underlying gabbro. Some
174 sheets are connected from below to sub-perpendicular pipe-like feeding structures (Fig. 3b
175 and c). In addition, when diapirs came near an overlying sheet, they could merge with it.
176 Alternatively, some diapirs did not intersect the overlying sheet but formed concave-down
177 structures (Fig. 3d). Except near Beg ar Fri, where an amphibole-rich cumulate has been
178 sampled (SJ44b, Fig. 2a), the gabbro is structurally and texturally homogeneous throughout
179 the Poul Rodou shoreline: no chilled margins, macrorhythmic units, or upward petrographic
180 gradation were observed.

181

182 3.2.2. *Saint-Jean's bay: monzogabbro-monzonite interactions*

183 The coast north of Saint-Jean-du-Doigt exposes spectacular and various monzogabbro-
184 (Q-)monzonite (see section 3.3 for rock nomenclature) interaction structures resulting from
185 brittle brecciation to mixing (producing hybrid rocks) through mingling (during which the
186 magmatic end-members retain their identity). At Saint-Jean's bay, angular breccias are
187 present only east of the dextral fault *F* (Fig. 1b) whereas mingling/mixing predominates
188 westward. Lobate structures are also visible in the transition zone to the Poul Rodou layered
189 gabbro-diorite unit.

190 Structures that result from ductile interactions between coexisting magmas include
191 pillowed mafic enclaves with chilled margins enclosed in a heterogeneous monzogabbro
192 (mingling, Fig. 4a), hybrid magmas (pure mixing), and banded rocks in the process of

193 hybridization (mingling/mixing, Fig. 4b). In partly hybridized rocks, several mafic enclaves
194 show diffuse margins. These interactions can be observed from microscopic (less than one
195 millimeter) to outcrop scales (several tens of meters). Locally, mafic enclaves present a
196 N40°E preferred orientation, suggesting ductile deformation in protoshear zones.

197 The angular facies consist of jigsaw-type breccias where polyhedral mafic enclaves are
198 enclosed in intermediate rocks forming a vein network (Fig. 4c). The veins are texturally
199 homogeneous intergranular (Q-)monzonites whereas a few blocky clasts exhibit
200 mixing/mingling features.

201

202 3.2.3. *Primel: cumulate-pegmatoid association*

203 Pegmatoids (gabbroic pegmatites), generally associated with plagioclase-phyric
204 cumulates, are distributed from Roc'h Louet to Primel (Fig. 1b). Cumulates are well exposed
205 at Roc'h Louet (Fig. 2b), whereas the coarsest-grained pegmatoid, containing large amphibole
206 crystals (up to 15 centimeters in length) and smaller plagioclase crystals, occurs westward
207 near the Primel red granite (Fig. 2c). There, pegmatoids occur as pods or veins within mafic
208 heteradcumulates with variable plagioclase contents. They are sometimes zoned, with an
209 amphibole-richer core. Pegmatoids are often more altered than the host gabbro. The cumulate-
210 pegmatoid association is bordered southward and southeastward by the monzogabbro-(Q-
211)monzonite unit of Saint-Jean. In this area, monzogabbros are locally rich in feldspar
212 megacrysts, similar to those described by Wiebe and Collins (1998) and Collins et al. (2006)
213 in the Devonian Kameruka Granodiorite (Bega batholith, southeastern Australia). Fine-
214 grained pegmatoids are found as patches or thin veins in mingled monzogabbro-(Q-
215)monzonite at Saint-Jean's bay western edge (Fig. 2b). In this zone, mottled pegmatoids have
216 also been observed. They are characterized by recrystallized amphibole-bearing flecks from 2
217 to 5 cm in diameter (see section 3.3).

218 Gabbroic aplites are often intimately associated with pegmatoids as patches or
219 irregular veinlets (Fig. 4d). They are distinct from the doleritic dykes, which display sharp
220 intrusive contacts with host rocks and have chilled margins.

221 In sample PM2 (Fig. 4d), an aplitic vein separates the pegmatoid from the cumulate,
222 the latter being edged by a dark reaction zone.

223

224 3.3. Petrology

225

226 According to the recommendations of the IUGS, the nomenclature of plutonic rocks is
227 based on modal compositions. As not all the primary phases are preserved, we have chosen to
228 use the R1-R2 chemical discrimination diagrams of La Roche et al. (1980), as utilized by
229 many authors (e.g., López-Moro and López-Plaza, 2004; Hellström et al., 2004).

230 At Poul Rodou, the SJIC rocks plot within the following fields of a R1-R2 diagram:
231 olivine gabbro; diorite, monzodiorite and (Q-)monzonite (sheets and diapirs); and granite
232 (intrusions). The Saint-Jean's bay samples plot as follow: olivine gabbro (doleritic dykes);
233 monzogabbro, monzonite, and Q-monzonite (mixing/mingling facies). At Primel, pegmatoids
234 are olivine gabbros. Associated cumulates plot as pyroxenite, a term not used here, given the
235 lack of modal pyroxene in the rocks. Following a similar line of argument (lack of olivine),
236 we prefer the term "gabbro" to "olivine gabbro".

237 The Primel cumulates mainly enclose labradorite, secondarily albitized, as a cumulus
238 phase (from 30 to 65 vol. %), with interstitial actinolite (which replaces oikocrysts, probably
239 of pyroxene), Fe-Ti oxides and apatite.

240 Pegmatoids are mainly composed of skeletal green hornblende and elongated albitized
241 plagioclase. Relics of diopside have been identified in a few samples. Small comb-shaped Fe-
242 Ti oxides, biotite and acicular apatite fill the spaces between the large crystals. The flecks of

243 the mottled pegmatoids on the western edge of Saint-Jean's bay contain Fe-Ti oxides,
244 amphibole and phyllosilicates. They might result from recrystallization of ancient oikocrystic
245 pyroxenes.

246 Gabbros and monzogabbros from the SJIC contain saussuritized plagioclase laths,
247 green hornblende, acicular actinolite, Fe-Ti oxides, apatite, biotite and sparse titanite and
248 zircon. Large oikocrysts of brown hornblende have been identified in several monzogabbro
249 samples. The dolerites are fine-grained and have a typical greenschist facies mineral
250 assemblage (albite, actinolite, epidote, chlorite).

251 The SJIC (Q-)monzonites are especially rich in andesine (up to 75 vol. %). The main
252 ferro-magnesian mineral is actinolite. The Q-monzonites, which are mainly located east of
253 Saint-Jean's bay, have more than 10 vol. % of quartz. Sheets and diapirs from the SJIC range
254 from diorite to Q-monzonite in composition. Sheets are rich in albitic plagioclase but also
255 contain amphibole (green hornblende and actinolite) with variable amounts of interstitial
256 quartz. Diapirs contain quartz, plagioclase, K-felspar and epidote.

257 Granites contain orthoclase, quartz, plagioclase, biotite, apatite and rare zircons.
258 Symplectitic quartz-feldspar associations are present in many SJIC granitic samples
259 (myrmekite).

260

261 **4. North-Guernsey Intrusive Complex (NGIC)**

262

263 *4.1. Geology*

264

265 Guernsey (Channel Islands), about 50 km off the French coast, is part of the
266 Armorican Massif (Fig. 1a). The island is divided into two main geological domains. The
267 Southern Metamorphic Complex mainly consists of Palaeoproterozoic gneisses (including the

268 Icart orthogneiss, with a magmatic U-Pb/zircon age of 2061 ± 2 Ma, Samson and D'Lemos,
269 1998), which were later intruded by the deformed Neoproterozoic Perelle Q-diorite (Samson
270 and D'Lemos, 1999). The Northern Neoproterozoic Intrusive Complex – hereafter referred to
271 as the North-Guernsey Intrusive Complex (NGIC) – is undeformed and partly composed of
272 layered rocks (Elwell et al., 1960, 1962; Bremond d'Ars, 1990; Bremond d'Ars et al., 1992).
273 The composite NGIC consists of four distinct units: the Saint Peter Port gabbro, the gabbro-
274 dioritic Bordeaux Group, the L'Ancrese granodiorite and the Cobo granite (Topley et al.,
275 1990; Fig. 1c). All these plutonic units were emplaced at the end of the Cadomian orogeny, at
276 about 560-550 Ma (Bremond d'Ars et al., 1992). The present study mainly deals with gabbro-
277 diorite layering in the Bordeaux Group (the Beaucette type in Bremond d'Ars et al., 1992) and
278 with the Spur Point cumulate-pegmatoid association (Saint Peter Port Gabbro). Alteration of
279 the NGIC rocks is generally moderate. Petrologic studies indicate that the Saint Peter Port
280 gabbro was emplaced under a lithostatic pressure of about 0.4 GPa (*c.* 12 km depth),
281 amphibole and plagioclase crystallized at about 940°C under relatively high oxygen fugacity
282 conditions, and magma water content ranged from 2 to 6 wt% (Bremond d'Ars et al., 1992).
283 The complex has a calc-alkaline affinity (Bremond d'Ars et al., 1992; see also section 5.2)
284 and belongs to the M-type Cadomian Granitoid Belt of Graviou and Auvray (1985).

285

286 *4.2. NGIC layering*

287

288 *4.2.1. Beaucette Marina: veined gabbroic macrorhythms*

289 The outcrops of the Beaucette Marina (gabbro-dioritic Bordeaux Group) show
290 partially cumulative macrorhythmic sequences, which are less than one to several meters
291 thick, and dip 20° westward (Fig. 2d, e and 5a, b, c). They are locally intruded by doleritic or
292 dioritic dykes. Each macrorhythm is composed of a gabbroic unit overlying a melagabbroic

293 unit. The base of a melagabbroic unit is generally fine-grained, as also observed by Elwell et
294 al. (1960). The transition from a melagabbroic unit to an overlying gabbroic one is
295 gradational, with amounts of phyrlic amphiboles decreasing upwards (see Fig. 9 insets in
296 section 5.1). Both units have an orthocumulate texture. While melagabbroic units are
297 petrologically homogeneous, the main gabbroic unit is formed by alternating dark and
298 mesocratic layers of a few centimeters thick (Fig. 5c) and is veined by leucocratic material,
299 forming an inter- and cross-connected network of centimeter-thick sheets, broadly parallel to
300 the layering (Fig. 5d).

301 Immediately below some melagabbroic units, thick evolved-gabbroic sheets are
302 observed, from which leucocratic pipes protrude upwards into the overlying melagabbros
303 (Fig. 5a, b). Such pipe-producing sheets also occur, more rarely, in the interior of the
304 melagabbroic units (Fig. 5a). They have a texture ranging from intergranular to
305 orthocumulative. The upper limit of the evolved-gabbroic sheets is irregular, sometimes
306 diffuse. Elwell et al. (1960) has described fine-grained margins in the upper part of some
307 gabbroic units at the contact with the pipe-producing sheets. All the leucocratic pipes are
308 inclined on average at about 30° from the main layering (Fig. 5e). They plunge toward the S-
309 SE. North of the area shown in Fig. 2e, two generations of neighboring pipes have distinct
310 pitches (c. 10° and 40° from the layering). Pipe compositions range from monzodiorite (this
311 study) to granodiorite (Elwell et al., 1960). In cross-section, the pipes are zoned, the core
312 being less differentiated than the rim (Fig. 5f; Elwell et al., 1960). The upper part of the pipes
313 is pegmatitic and the host rocks are systematically altered near the pegmatitic zones (Fig. 5f).
314 Elwell et al. (1960) have described two spots where pipes join with the overlying cross-
315 connected dioritic vein system.

316

317 *4.2.2. Spur Point: cumulate-pegmatoid association*

318 The Saint Peter Port gabbro is a 0.8 km-thick layered slab, gently dipping westward
319 (Briden et al., 1982). It is composed of three main rock types (Bremond d'Ars et al., 1992).
320 The most spectacular of which is the mottled orthocumulate of Spur Point, characterized by
321 layers of poikilitic amphibole crystal flecks (Roach, 1971; Bremond d'Ars, 1990; Bremond
322 d'Ars et al, 1992; Fig. 6a, b). This facies has been interpreted as a boundary layer cumulate
323 (Bremond d'Ars et al, 1992).

324 Pegmatoidic rocks crop out at Spur Point (Fig. 6c). Their mineralogy and texture are
325 similar to those in the SJIC. However, here in the NGIC, cumulates associated with
326 pegmatoids are mottled.

327

328 *4.3. Petrology*

329

330 In a R1-R2 diagram (La Roche et al., 1980), Beaucette's rocks are gabbronorite
331 (melagabbroic units), olivine gabbro (gabbroic units and pipe-producing sheets), diorite
332 (dykes and cross-connected veins), and monzodiorite (pipes). As for Primel (SJIC), the Spur
333 Point cumulates plot as pyroxenite, a term not used here.

334 The Spur Point mottled orthocumulates contain cumulus calcic plagioclase (An 80)
335 and clinopyroxene (Fig. 6b). The intercumulus phases are clino- and orthopyroxene,
336 amphibole (hastingsite), Fe-Ti oxides and apatite. The flecks correspond to large oikocrystic
337 amphiboles.

338 The NGIC pegmatoids are composed of large skeletal green hornblende, elongate
339 albitized plagioclase, comb-shaped Fe-Ti oxides, biotite and acicular apatite.

340 Gabbroic and granitic rocks have also mineralogies comparable to those of the SJIC
341 gabbros and granites. The melagabbros (gabbronorites) show green hornblende as cumulus

342 phase (< 50 vol. %), as well as plagioclase, Fe-Ti oxides, apatite and biotite. We have also
343 noted the presence of clots of small amphibole grains in these rocks.

344 In Beaucette, the dioritic veins, sheets and dykes are mainly composed of plagioclase,
345 hornblende and biotite, whereas the monzo/granodioritic pipes are rich in plagioclase, K-
346 feldspar, green hornblende and, occasionally, quartz and clinopyroxene. The sheet sample
347 GS13a is composed of *c.* 30 % of 2 mm-long zoned plagioclase, as cumulus phase.
348 Concentrations of acicular hornblende are observed where pipes connect overlying cross-
349 connected dioritic veins (Elwell et al., 1960).

350 The pipe-producing evolved gabbroic sheet sample GS13a from Beaucette and the
351 mottled orthocumulate sample GS1a from Spur Point are both characterized by cumulus An-
352 rich plagioclase (An 60-90; Fig. 7a). No other analyzed NGIC sample shows such a
353 characteristic. A chemical profile across such a plagioclase crystal (sample GS1a, Fig. 7b)
354 reveals a calcic mantle (An 60-75) comprised between an An-rich core (An 75-90) and an An-
355 poor margin (An 40-55). This mineralogical specificity will be discussed in section 6.3.1.

356

357 **5. Geochemistry**

358

359 *5.1. Geochemical sections through gabbro-diorite units*

360

361 Vertical variations of MgO, TiO₂ and Al₂O₃ through four gabbro-dioritic sections are
362 shown in Figs 8 (SJIC) and 9 (NGIC). The chemical composition of the Poul Rodou gabbro is
363 relatively constant, above and below the diapir-producing leucocratic sheets, for all the
364 sections (Fig. 8). Only TiO₂ varies significantly, from 1.18 (SJ34g) to 1.91 wt% (SJ43f). This
365 relative chemical homogeneity of the mafic body is a rather original feature with respect to
366 many other MASLs (e.g., Wiebe, 1996). By contrast, the macrorhythmic sequences of the

367 NGIC display variable compositions (Fig. 9). Melagabbros are highly magnesian, with MgO
368 contents up to 14.35 wt% (GS10d). MgO is slightly higher in the lower part of the
369 melagabbroic units (GS7a versus GS7d in Fig. 9). Gabbroic units are more heterogeneous and
370 less magnesian ($5 < \text{MgO} < 10$ wt%, Fig. 9). The leucocratic veins, sheets and diapirs/pipes
371 display various compositions. In both intrusions, the diapirs/pipes are systematically more
372 evolved than the sheets from which they are extracted (SJ34b1 versus SJ34c; GS10c versus
373 GS13a; Table 1 and Figs 8 and 9). However, parts of some sheets are more differentiated than
374 some diapirs. For example, the upper part of the sheet SJ43c is more evolved than the diapir
375 SJ34b1, which relates to another sheet (Table 1 and Fig. 8).

376

377 *5.2. Trace elements*

378

379 Trace elements which are both incompatible and immobile can be used to determine
380 the magmatic affinity of the mafic rocks. In the La/10-Y/15-Nb/8 diagram (Fig. 10) of
381 Cabanis and Lecolle (1989), the SJIC gabbros and monzogabbros plot mainly in the E-MORB
382 field whereas the gabbros and melagabbros from the NGIC clearly have a calc-alkaline
383 affinity.

384 The chondrite-normalized rare earth element (REE) field of the Poul Rodou gabbros
385 (SJIC) is shown in Fig. 11a, with REE patterns of two leucocratic sheets and related diapirs.
386 The sheet and diapir SJ34 are moderately differentiated. The diapir SJ34b1 is slightly
387 enriched in light REE (LREE) and depleted in heavy REE (HREE) with respect to the
388 corresponding sheet SJ34c, which plots above the gabbroic field. The sheet sample SJ43c
389 shows lower REE concentrations than the less differentiated sheet sample SJ34c. The diapir
390 SJ43d is enriched in LREE and depleted in HREE with respect to its parental sheet SJ43c.
391 Both have positive Eu anomalies.

392 The REE patterns of some other rocks representative of the SJIC are exhibited in Fig.
393 11b. Pattern similarities between the diapir SJ34b1 and the monzonite SJ9 (mingling zone at
394 Saint-Jean's bay) and between the evolved sheet SJ43c and the Q-monzonite SJ17 (vein in
395 breccia with angular clasts at Saint-Jean's bay) are noticeable. The pegmatoid SJ16 is less rich
396 in REE than the gabbros. Of all the samples, cumulates have the lowest REE contents. With
397 respect to the monzonite SJ9, the granite SJ22 is enriched in Ce and HREE, and displays a
398 large negative Eu anomaly.

399 In the NGIC, all the samples from the macrorhythmic sequences have parallel patterns
400 (Fig. 11c). This is also the case for the pipe-producing gabbroic sheet GS13a, located near the
401 upper limit of the gabbroic REE field. By contrast, the thin dioritic sheet GS7c and the
402 monzodioritic pipe GS10c are highly depleted in HREE with respect to GS13a. Although
403 contents of La, Eu and Yb are equal in GS10c and GS7c, GS10c has a concave-up shaped
404 pattern indicating depletion in Middle REE (with the exception of Eu).

405 The gabbroic pipe-producing sheet GS13a and the mottled cumulate of Spur Point
406 GS1a, which contain An-rich plagioclase phenocrysts (An 60-90; Fig. 7), display cross-
407 cutting REE curves, with comparable Eu contents (Fig. 11d). The Cobo granite GS8 has a
408 concave-up pattern and a negative Eu anomaly.

409

410 5.3. *Isotopes*

411

412 The Sr and Nd isotopic data and analytic details are shown in Table 2. The range of
413 the NGIC $^{87}\text{Sr}/^{86}\text{Sr}$ initial ratios is very restricted (0.7055 to 0.7058), regardless of the rock
414 type (data from Bremond d'Ars et al., 1992). In the SJIC, mafic rocks (gabbros, pegmatoids,
415 and dolerites) exhibit the most positive ϵ_{Nd} values at 347 Ma (+4.7 to 5.9) and initial Sr ratios
416 between 0.7039 and 0.7049. These values are similar to those obtained by Barboni et al.

417 (2010) on pseudo-adakites related to the SJIC (+2.9 to + 6.8 and 0.7038 to 0.7047). The
418 intermediate SJIC rocks (monzogabbros, monzonites, Q-monzonites, and diorite) have less
419 positive ϵ_{Nd} values (+2.4 to +3.2) and initial Sr ratios which range from 0.7043 to 0.7069.
420 This scattering suggests that the Rb-Sr system was not closed. The granite sample SJ22 also
421 exhibits a positive ϵ_{Nd} value at 347 Ma (+3.0) and a low initial Sr ratio (<0.700) which also
422 shows open system behavior for Rb-Sr. A noticeable feature is the sharp isotopic contrast
423 between the Poul Rodou gabbro SJ34a (+5.9) and the dioritic sheet SJ34c (+2.6), two
424 neighbor samples separated by *c.* 3 m (Fig. 3a and 8).

425 It follows that the gabbro and the leucocratic sheets from Poul Rodou are not
426 cogenetic. The source of the former corresponds to that of the doleritic dykes and peripheral
427 pegmatoids, whereas the Poul Rodou sheets (and diapirs) have an isotopic composition
428 comparable to that of the other SJIC intermediate rocks.

429

430 **6. Discussion**

431

432 *6.1. A review*

433

434 *6.1.1. MASLI-type reservoirs: the models*

435 Wiebe and others have defined the concept of MASLI and studied many examples of
436 such intrusions, especially in Maine. A MASLI petrologically corresponds to a composite
437 layered sequence of alternating gabbroic and dioritic units situated between or below granitic
438 bodies (Chapman and Rhodes, 1992; Wiebe, 1996; Wiebe and Collins, 1998). Variants are
439 intrusions of bimodal gabbro-diorite (e.g., Ingonish, Cape Breton Island: Wiebe, 1974) or
440 diorite-granite (e.g., Nord-Forez, Massif Central, France: Barbarin, 1988), which display
441 some of the characteristic features of MASLIs. These complexes are interpreted to be the

442 result of repeated mafic intrusions in a crystallizing dioritic/granitic reservoir (Wiebe, 1974,
443 1993b, 1996). This group of models is supported, among other things, by the observation of
444 pillow-like bodies of chilled gabbro in intermediate/felsic rocks (Wiebe, 1993b; Wiebe et al.,
445 2001). Diorites are generally viewed either as products of fractional crystallization of the
446 gabbro, or as resident cumulates.

447 A multistep model for the Isle au Haut Maine igneous complex (Maine), similar to
448 those of Wiebe and others, was proposed by Chapman and Rhodes (1992). The model
449 accounts for the formation of a layered sequence of ten alternating (tholeiitic) gabbroic and
450 dioritic units of magmas, which were contemporaneous. The bases of the gabbros are chilled
451 against the underlying diorites. The authors state that mafic liquids were periodically
452 emplaced into a silicic magma chamber at the rheological transition from a relatively felsic
453 cumulate to an overlying felsic magma. Each gabbroic unit is injected below a dioritic liquid,
454 but above a solidifying dioritic crystal mush, as expected from the magma density contrast.
455 Once emplaced, crystallization progresses in the underlying dioritic mush and produces Q-
456 monzodioritic sheets and pipes, which intrude the gabbroic layer. Diapirs are subsequently
457 produced from the crystallizing sheets.

458 The development of such gravity-driven instabilities in layered magmas have been
459 modeled and applied to the NGIC (Bremond d'Ars, 1990; Bremond d'Ars and Davy, 1991).
460 However, according to these authors, it is not clear whether the sheets in the NGIC result
461 from intrusions within the gabbros, or the reverse. The opinion of Wiebe (1993b) is that “the
462 ‘veins’ in Guernsey have textures and compositions that are appropriate for feldspar
463 cumulates, not solidified liquids”. He views the NGIC as a crystallizing intermediate/felsic
464 reservoir periodically invaded by mafic liquids.

465

466 *6.1.2. Cumulates and pegmatoids*

467 The connection between mafic cumulates, gabbroic pegmatites (pegmatoids) and
468 aprites has been established by many authors. For instance, Beard and Day (1986) published a
469 thorough study of such rocks in the Smartville intrusive complex, Sierra Nevada, California.
470 They pointed out the following features: (i) the pegmatoids occur as pods and segregations in
471 gabbroic rocks; (ii) they are often found in association with fine-grained aprite of similar
472 mineral assemblage; and (iii) they have a very mafic composition, as observed by other
473 authors (e.g., McBirney and Noyes, 1979). Contrary to previous authors who proposed
474 subsolidus processes (e.g., Bow et al., 1982), Beard and Day (1986) favour that rocks form by
475 *in situ* crystallization. They envisage that a mafic intercumulus melt is extracted from a
476 cumulate stack in the presence of a fluid phase. The process could be enhanced by the
477 disruption of the cumulate assemblage due to a drop in the confining pressure. This model is
478 consistent with the one proposed by Momme and Wilson (2002) for the Kraemer Island
479 macrodyke, Greenland. It is also similar to the model of pegmatoid formation in thick basaltic
480 lava flows proposed by Caroff et al. (1997). An alternative model suggests that the pegmatoid
481 crystals grew by reaction between primary mafic mineral grains and a superheated liquid
482 possibly resulting from a pressure drop (Cawthorn and Boerst, 2006). In a plumbing system
483 connected to the surface, a pressure drop can easily be achieved subsequent to an eruption. In
484 an intrusion, confined at depth within deformable host rocks, only a volumetric expansion of a
485 constant mass plumbing system could also induce a pressure drop.

486

487 6.2. Layering and diapirism in the SJIC and NGIC

488

489 Both SJIC and NGIC display comparable characteristics, which justifies the present
490 combined study: (1) both intrusions are triple-component MASLIs (gabbro, diorite and
491 granite); (2) pegmatoids occur in association with mafic cumulates, especially at the edges of

492 both complexes; (3) a lateral or basal part of the intrusions is formed by gabbroic sequences
493 interlayered with dioritic sheets producing diapirs. Nevertheless, numerous contrasted features
494 lead us to propose two different models for the construction of the gabbro-dioritic layered
495 sequences.

496

497 6.2.1. *Melagabbros and gabbros*

498 Two noticeable features of the NGIC gabbro-dioritic unit not observed in the SJIC are
499 the presence of macrorhythms and modal layering within the gabbroic sequences. This
500 petrological heterogeneity induces geochemical variations (Fig. 9 and 11c) and suggests
501 crystal accumulation. By contrast, the tholeiitic Poul Rodou gabbro (SJIC) is relatively
502 homogeneous (Fig. 11a). Therefore, it is probably not a cumulate, but was rather a liquid that
503 crystallized *in situ* without significant crystal settling, possibly after a period of convection.
504 For instance, Philpotts et al. (1996) have shown that tholeiitic magmas, when only one-third
505 crystallized, can form crystal mushes dominated by thin laths of plagioclase and elongated
506 pyroxene grains. In such magmas, an interlocking network of crystals can form at low solid
507 content (possibly only 20%), precluding any further convection and crystal settling. Such a
508 model is consistent with both the tholeiitic affinity of the Saint-Jean gabbro (Fig. 10) and the
509 rock textures, which are intergranular to oikocrystic. On the contrary, the rhythmic sequences
510 of the calc-alkaline NGIC, and the orthocumulate texture fit with a crystal accumulation
511 model.

512 In Fig. 12, we propose two models to explain the formation of the gabbro-dioritic
513 layered sections of the SJIC and NGIC. The Poul Rodou gabbro is purported to be a simple
514 network-type crystal mush, crystallizing from the base up (Fig. 12a, b, c). In Beaucette, each
515 melagabbro/gabbro pair is asserted to correspond to a mafic recharge (Fig. 12d, g), having
516 undergone two successive crystal-settling events. At first, settling involves only mafic crystals

517 (olivine, pyroxene \pm primary hornblende: Fig. 12e) and next, plagioclase appears on the
518 liquidus (Fig. 12f). In the first step, densities of the mafic crystals are comparable and the
519 resulting cumulate is highly mafic and texturally homogeneous (melagabbroic unit). With the
520 appearance of plagioclase, the density difference between feldspar and mafic crystals can
521 produce alternating dark/mesocratic layers (gabbroic unit), according to the model of Sparks
522 et al. (1993).

523

524 6.2.2. Formation of leucocratic sheets and diapirs

525 Models of dioritic/monzonitic reservoirs periodically replenished by mafic liquids
526 hardly apply to all the stages of construction of both intrusions.

527 *In the SJIC*, observations supporting the idea that intermediate magmas have invaded
528 mafic ones include: (1) the several sheets of intermediate composition that we interpret as
529 intrusions in the Poul Rodou homogeneous gabbro; (2) the monzonitic dykes throughout most
530 of Saint-Jean's bay, especially those including angular mafic breccias (Fig. 4c); (3) the lack of
531 evidence for chilling of the Poul Rodou gabbro against the dioritic sheets (Fig. 8); and (4) the
532 large predominance of the gabbroic rocks over the whole intrusion. We do not exclude that
533 mafic inputs, at huge rates, possibly inducing intensive thermal rejuvenation of a more felsic
534 resident magma, were previously involved in the SJIC. We mean here that, as observed today,
535 (1) and (2) are unlikely the direct, *in situ* or slightly displaced, remnants of an initial felsic
536 reservoir that remains rather hypothetical from (3) and (4).

537 The chilled gabbroic pillow-like enclaves, such as those of Fig. 4a, result from
538 fragmentation of mafic magmas in more felsic ones. Such a mingling is controlled by
539 rheological contrasts and/or surface energy and depends on the relative volumes and
540 temperatures of available magmas (e.g., Sparks and Marshall, 1986; Fernandez and Barbarin,
541 1991; Hallot et al., 1996; Pons et al., 2006). Thus, it can be achieved during or just after new

542 mafic inputs, but may alternatively result from convective motions in the interior of a large
543 composite reservoir or from injections of an external more felsic magma into a resident mafic
544 magma. Chilling of the latter just requires significant volumes of colder, but still mobile,
545 more felsic magmas.

546 Therefore, we propose a model of a reservoir repeatedly replenished by dioritic
547 magmas for the SJIC. Those magmas were not genetically related, nor had they to be initially
548 at the same temperature. In the reservoir, the gabbroic magma density increases downward
549 with cooling, hence crystallinity. Andesites/diorites and basalts/gabbros may have comparable
550 densities, especially when they are of tholeiitic affinity (e.g., Sparks et al., 1980; Sparks and
551 Huppert, 1984; Caroff, 1995). A partly crystallized dioritic magma rising through a tholeiitic
552 gabbro crystallizing from below is thus expected to be buoyant initially, then at neutral
553 buoyancy and finally denser than the gabbroic magma. In Fig 12a and b, a 950°C dioritic
554 magma with 30% plagioclase phenocrysts enters a gabbroic reservoir crystallizing from
555 below. At the base (1), the gabbroic magma is 70% solid at 1100°C. At upper levels (2) and
556 (3), it is 30% solid at 1150°C and liquid at 1200°C, respectively (all values are approximates).
557 Reaction kinetics being much slower than heat transfer, a metastable dioritic melt plus
558 crystals at thermal equilibrium with the resident magma is considered at these levels.
559 Densities were estimated given that the density of a liquid, obtained from Bottinga and Weill
560 (1970), is about 90% of that of its solid equivalent and assuming that this ratio applies to the
561 solid fraction whatever it is (Fig. 12). The results show that at levels (1) and (2), a gabbroic
562 magma remains denser than a dioritic magma. At level (3), equidensity is reached allowing a
563 dioritic magma to spread out, forming sheets. Thus, we interpret each SJIC sheet as the result
564 of some horizontal emplacement of porphyric magmas of intermediate composition into
565 poorly crystallized gabbros at levels of neutral buoyancy. Late felsic diapirs formed at the top
566 of emplaced sheets while the equidensity front moved upward as cooling proceeded (Fig. 12b

567 and c). *In situ* fractionation within the sheets favored the late production of low density
568 magmatic liquids. The REE patterns of the diapirs are depleted in HREE with respect to the
569 sheets from which they were extracted (Fig. 11a). This is consistent with fractionation of a
570 significant amount of amphibole within the sheets. Indeed, amphibole preferentially
571 incorporates middle to heavy REE relative to LREE (e.g., Caroff et al., 1999).

572 *In the NGIC*, dioritic sheet and vein geometries are controlled by the macrorhythms:
573 the pipe-producing sheets are generally located along the lower boundary of the melagabbroic
574 units and the cross-connected dioritic vein network forms in the gabbroic units according to
575 the framework of the dark/mesocratic layers. These features suggest that the gabbroic
576 structures existed prior to the dioritic veining. The fine-grained margins at the base of
577 melagabbroic units relate to mafic replenishments before the dioritic invasion.

578 The main similarity between the SJIC and the NGIC was the late influx of the dioritic
579 magmas with respect to the main gabbroic magmas. At Beaucette, both magmas were close to
580 isotopic equilibrium. The emplacement of the dioritic sheets was not directly controlled by
581 density ratios, but rather by pre-existent rhythmic structures within cumulates (Fig. 12h). Two
582 groups of sheets have to be distinguished. An initial gabbroic to dioritic magma was emplaced
583 just beneath the base of the melagabbroic units (Fig. 5a, c). The sheet-derived pipes cut across
584 the melagabbroic unit (Fig. 5b), until the overlying gabbroic unit. The concave-up shape of
585 the REE pattern of the pipe GS10c (Fig. 11c) is consistent with crystallization and
586 fractionation of both amphibole and apatite in its parental sheet (Caroff et al., 1999). Relative
587 motions between the unconsolidated/mushy units possibly caused the vertical pipes to become
588 inclined (Fig. 5e, 12i), as previously proposed by Elwell et al. (1960). They might have
589 created proto-fissures in the gabbroic unit and thus have favored the emplacement of the
590 (monzo)dioritic second group of sheets, which are cross-connected and fed by the pipes (Fig.
591 5d, 12i). The gabbroic layering, seen as controlling the architecture of the cross-connected

592 vein/sheet network, supports our interpretation of late dioritic invasion within gabbros.
593 Cumulative features of the sheets reveal that the invading magmas possibly contained
594 plagioclase phenocrysts, such as those in the SJIC.

595

596 *6.3. Variations in the mode of MASLI construction*

597

598 Our models (Fig. 12) agree with the general physical conditions and the mechanisms
599 by which layers, pipes, diapirs and other plutonic structures are supposed to form within
600 crystallizing magmas (e.g., see Barbey, 2009 and Patterson, 2009 and references therein for
601 recent reviews). In our opinion, the SJIC and the NGIC support the general idea that
602 intermediate/felsic replenishment of a mafic reservoir is a situation much more common than
603 previously thought, though not as common as mafic replenishment.

604

605 *6.3.1. NGIC*

606 Bremond d'Ars et al. (1992) have proposed a sketchy model of the NGIC reservoir.
607 According to these authors, the layered rocks (Saint-Peter Port cumulate and Beaucette-type
608 gabbro-diorite) formed near the margin of the chamber, by upwards prograding crystallization
609 and replenishments. The present dip of the layers is primary. Far from the margins, the centre
610 of the reservoir was probably convective, which explains the lack of layering in most of the
611 Bordeaux gabbro-diorite outcrops, with the exception of Beaucette. The peripheral granitic
612 bodies (Cobo, L'Ancrese) are proposed to form by mixing and assimilation of crust-derived
613 melts with the gabbro-diorite magmas. Large volumes of mafic magma are thought to have
614 induced melting of country rocks at depth within the plumbing system.

615 We agree with the basic ideas of this model, except for the the hypothesis of crustal
616 melting. Although interactions between gabbro-dioritic and granitic rocks are undeniable

617 (Topley et al., 1982; D'Lemos, 1996), available isotopic data seems hardly consistent with
618 crustal melting (Table 2). We rather suggest, as D'Lemos (1996), that at least the Cobo
619 granite is to a great extent cogenetic with the Bordeaux gabbro-diorite, as it is often observed
620 in MASLIs (e.g., Wiebe, 1993a, b, 1994, 1996; Wiebe and Collins, 1998).

621 An-rich plagioclases in both the mottled cumulate GS1a from Spur Point and the
622 gabbroic sheet sample GS13a from Beaucette support the hypothesis that the invading dioritic
623 liquid(s) originate(s) from the mottled Saint-Peter-Port/Spur Point cumulate, interpreted as a
624 boundary layer by Bremond d'Ars et al. (1992). An-rich plagioclase cores ($An > 75$, Fig. 7b)
625 suggest crystallization under hydrous conditions (Cordier et al., 2007). Derivation of a
626 GS13a-type composition from a liquid leaving a GS1a-type cumulate is also supported by
627 trace element compositions. Indeed, cross-cutting REE curves in Fig. 11d possibly reflect
628 crystal fractionation/accumulation (plagioclase, amphibole and/or apatite).

629

630 6.3.2. *SJIC*

631 A model of the SJIC is drawn in Fig. 13.

632 Granitic intrusions (Fig. 2a) have emplaced during or just after the crystallization of
633 the gabbro-dioritic magmas.

634 Pegmatoids and associated mafic cumulates are located near the edge of the complex
635 (Fig. 1b and 2b, c). With an isotopic composition close to that of the Poul Rodou gabbro and
636 the doleritic dykes, but more mafic, pegmatoids likely correspond to liquids issued from a
637 mafic intercumulus melt in the presence of a fluid phase. Melt extraction might have been
638 enhanced by the disruption of the cumulate stack, perhaps in a context of drop of the
639 confining pressure (Beard and Day, 1986; Momme and Wilson, 2002). Reactions of the liquid
640 with primary mafic minerals of the cumulate might explain Mg-rich pegmatoid compositions
641 (Cawthorn and Boerst, 2006).

642 Mixing and mingling seem to have preferentially occurred in the central part of the
643 reservoir. Dioritic liquids (in a broad sense) mix with gabbroic magmas to form variable
644 hybridized products, the isotopic composition of which tends toward that of the diorites. The
645 most homogeneous hybridized product, which has a dioritic isotopic signature (Table 2),
646 corresponds to the Saint-Jean's bay monzogabbro. Such an isotopic homogenization in a
647 MASLI, by mixing and diffusion (Steward and De Paolo, 1992), has already been described
648 by Waight et al. (2007). Angular breccias, also drawn in Fig. 13, can result either from
649 gabbro/diorite interactions in a more peripheral (i.e. colder) region of the reservoir, or,
650 alternatively, from late arrivals of dioritic liquids in a solidifying magma. The ductile to brittle
651 behavior of a magma which can be inferred from the preserved shapes of the enclaves also
652 depends on the strain rates involved during fragmentation (Fernandez and Gasquet, 1994;
653 Hallot et al., 1996; Petford, 2009).

654 At Poul Rodou, the isotopic composition of the felsic sheets differs from that of the
655 enclosing resident gabbro. The SJIC intermediate and felsic products are therefore issued
656 from a source which is different from that of the Poul Rodou gabbro / Primel pegmatoid /
657 Saint-Jean dolerite group. An AFC-type crustal contamination of the felsic liquid in a deep
658 reservoir possibly accounts for such features.

659

660 **7. Conclusions**

661

662 (1) The Saint-Jean-du-Doigt (SJIC) and the North-Guernsey (NGIC) Intrusive
663 Complexes are two Mafic-Silicic Layered Intrusions (MASLI) of the armorican Massif. Both
664 are triple component complexes (gabbro, diorite, granite) characterized by the occurrence of
665 pegmatoids in association with cumulates and of gabbroic units including diapir-producing

666 dioritic sheets. The NGIC is Cadomian and calc-alkaline. Mafic rocks of the Hercynian SJIC
667 are tholeiitic.

668 (2) Pegmatoids are interpreted as liquids extracted from a mafic intercumulus melt in
669 the presence of a fluid phase, subsequent to the disruption of a peripheral cumulate stack,
670 possibly during a drop of the confining pressure.

671 (3) At least at some stages, the gabbro-dioritic units of the SJIC and the NGIC can
672 both result from repeated influxes of magmas of intermediate composition within mafic
673 reservoirs, but they are built differently. The SJIC gabbro could result from *in situ*
674 crystallization of a relatively uniform magma in which crystal settling was not significant.
675 Assuming they were metastable, dioritic magmas could have risen as gravity-driven diapirs in
676 such a crystallizing gabbro before they spread to form sheets at levels of neutral buoyancy. By
677 contrast, the NGIC gabbros correspond to cumulates. At Beaucette, they display a rhythmic
678 layering which has guided the subsequent dioritic injections.

679

680 **Acknowledgements**

681 We are grateful to P.-M. Le Dantec for field assistance (Primel and Roc'h Louet
682 cartography). Detailed and constructive comments by Dr P. Barbey and an anonymous
683 reviewer helped us to improve the manuscript. Pertinent suggestions of A. Brink are
684 gratefully acknowledged. We also thank Dr C.G. Barnes for discussions and Dr N. Eby for
685 editorial assistance.

686

687 **References**

688

689 Auvray, B., Charlot, R., Vidal, P., 1980. Données nouvelles sur le protérozoïque inférieur du
690 domaine nord-armoricain (France) : âge et signification. *Canadian Journal of Earth*
691 *Sciences* 17, 532-538.

692 Barbarin, B., 1988. Field evidence for successive mixing and mingling between the Piolard
693 Diorite and the Saint-Julien-la-Vêtre Monzogranite (Nord-Forez, Massif Central,
694 France). *Canadian Journal of Earth Sciences* 25, 49-59.

695 Barbey, P., 2009. Layering and schlieren in granitoids: a record of interactions between
696 magma emplacement, crystallization and deformation in growing plutons. *Geologica*
697 *Belgica* 12, 109-133.

698 Barboni, M., Bussy, F., Schoene, B., Schaltegger, U., 2008. Architecture and emplacement
699 mechanism of the Saint Jean du Doigt bimodal intrusion, Brittany, France. *Geophys.*
700 *Res. Abstr.* 10, EGU2008-A-05182.

701 Barboni, M., Bussy, F., Chiaradia, M., 2010. Origin of Early Carboniferous pseudo-adakites
702 in northern Brittany (France) through massive amphibole fractionation from hydrous
703 basalt. *Terra Nova*, doi:10.1111/j.1365-3121.2010.00974.x.

704 Beard, J.S., Day, H.W., 1986. Origin of gabbro pegmatite in the Smartville intrusive
705 complexe, northern Sierra Nevada, California. *American Mineralogist* 71, 1085-1099.

706 Bottinga, Y., Weill, F., 1970. Densities of liquid silicate systems calculated from partial molar
707 volumes of oxide components. *American Journal of Science* 269, 169-182.

708 Bow, C., Wolfgram, D., Turner, A., Barnes, S., Evans, J., Zdepski, M., Boudreau, A., 1982.
709 Investigations of the Howland reef of the Stillwater Complex, Minneapolis adit area :
710 stratigraphy, structure, and mineralization. *Economic Geology* 77, 1481-1492.

711 Bremond d'Ars, J. de, 1990. Estimation des propriétés rhéologiques des magmas par l'étude
712 des instabilités gravitaires. *Pétrologie du complexe plutonique de Guernesey. Mémoires*

713 et Documents du Centre Armoricaïn d'Etude Structurale des Socles (Thesis), Rennes 35,
714 370 p.

715 Bremond d'Ars, J. de, Davy, P., 1991. Gravity instabilities in magma chambers – rheological
716 modeling. *Earth and Planetary Science Letters* 105, 319-329.

717 Bremond d'Ars, J. de, Martin, H., Auvray, B., Lécuyer, C., 1992. Petrology of a magma
718 chamber: the plutonic complex of Guernsey (Channel Islands, UK). *Journal of the*
719 *Geological Society of London* 149, 701-708.

720 Briden, J.C., Clark, A., Fairhead, J.D., 1982. Gravity and magnetic studies in the Channel
721 Islands. *Journal of the Geological Society of London* 139, 35-48.

722 Cabanis, B., Lecolle, M., 1989. Le diagramme La/10-Y/15-Nb/8: un outil pour la
723 discrimination des séries volcaniques et la mise en évidence des processus de mélange
724 et/ou de contamination crustale. *Comptes Rendus de l'Académie des Sciences de Paris*
725 309, série II, 2023-2029.

726 Capdevila, R., 2010. Les granites varisques du Massif armoricaïn. *Bulletin de la Société*
727 *Géologique et Minéralogique de Bretagne (D)* 7, 1-52.

728 Caroff, 1995. Open system crystallization and mixing in two-layer magma chambers. *Lithos*
729 36, 85-102.

730 Caroff, M., Ambrics, C., Maury, R.C., Cotten, J., 1997. From alkali basalt to phonolite in
731 handsized samples: vapor-differentiation effects in the Bouzentès lava flow (Cantal,
732 France). *Journal of Volcanology and Geothermal Research* 79, 47-61.

733 Caroff, M., Guillou, H., Lamiaux, M., Maury, R.C., Guille, G., Cotten, J., 1999. Assimilation
734 of ocean crust by hawaiitic and mugearitic magmas: an example from Eiao (Marquesas).
735 *Lithos* 46, 235-258.

736 Cawthorn, R.G., Boerst, K., 2006. Origin of the pegmatitic pyroxenite in the Merensky Unit,
737 Bushveld Complex, South Africa. *Journal of Petrology* 47, 1509-1530.

738 Chantraine, J., Chauris, L., Cabanis, B., Chauris, M.-M., Larsonneur, C., Herrouin, Y., Rabu,
739 D., Lulzac, Y., Bos, P., 1986. Notice explicative, carte géol. France (1/50 000), feuille
740 Plestin-Les-Grèves (202). Orléans, BRGM, 84 p. Geological map by J. Chantraine *et al.*
741 (1985).

742 Chapman, M., Rhodes, J.M., 1992. Composite layering in the Isle au Haut Maine igneous
743 complex, Maine: Evidence for periodic invasion of a mafic magma into an evolving
744 magma reservoir. *Journal of Volcanology and Geothermal Research* 51, 41-60.

745 Coint, N., Caroff, M., Hallot, E., Peucat, J.J., 2009. The gabbro-diorite layered intrusions of
746 Saint-Jean-du-Doigt (France) and Beaucette (Guernsey, Channel Island), Armorican
747 Massif: an emplacement model. *Geological Society of America Abstracts with*
748 *Programs* 41 (2), 30.

749 Coint, N., Hamelin, C., Caroff, M., 2008. Le complexe gabbro-dioritique lité de Saint-Jean-
750 du-Doigt, Massif armoricain: un exemple de réservoir magmatique de type MASLI.
751 *Bulletin de la Société Géologique et Minéralogique de Bretagne (D)* 5, 1-29.

752 Collins, W.J., Wiebe, R.A., Healy, B., Richards, S.W., 2006. Replenishment, crystal
753 accumulation and floor aggradation in the megacrystic Kamberuka suite, Australia.
754 *Journal of Petrology* 47, 2073-2104.

755 Cordier, C., Caroff, M., Juteau, T., Fleutelot, C., Hémond, C., Drouin, M., Cotten, J.,
756 Bollinger, C., 2007. Bulk-rock geochemistry and plagioclase zoning in lavas exposed
757 along the northern flank of the Western Blanco Depression (Northeast Pacific): Insight
758 into open-system magma chamber processes. *Lithos* 99, 289-311.

759 Cotten, J., Le Dez, A., Bau, M., Caroff, M., Maury, R., Dulski, P., Fourcade, S., Bohn, M.,
760 Brousse, R., 1995. Origin of anomalous rare-earth element and yttrium enrichments in
761 subaerial exposed basalts: Evidence from French Polynesia. *Chemical Geology* 119,
762 115-138.

- 763 De Paolo, D.J., 1988. Neodymium isotope geochemistry, an introduction. Mineral and rocks,
764 20. Springer Verlag, Berlin, Heidelberg.
- 765 D'Lemos, R.S., 1996. Mixing between granitic and dioritic crystal mushes, Guernsey,
766 Channel Islands, UK. *Lithos* 38, 233-257.
- 767 Elwell, R.W.D., Skelhorn, R.R., Drysdall, A.R., 1960. Inclined granitic pipes in the diorites of
768 Guernsey. *Geological Magazine* 97, 89-105.
- 769 Elwell, R.W.D., Skelhorn, R.R., Drysdall, A.R., 1962. Net veining in the diorite of north east
770 Guernsey, Channel Islands. *Journal of Geology* 70, 215-226.
- 771 Fernandez, A.N., Barbarin, B., 1991. Relative rheology of coeval mafic and felsic magmas :
772 Nature of resulting interaction processes and shape and mineral fabrics of mafic
773 microgranular enclaves. In: Didier, J., Barbarin, B. (Eds), *Enclaves and granite
774 petrology*. Elsevier, Amsterdam, p. 263-275.
- 775 Fernandez, A.N., Gasquet, D.R., 1994. Relative rheological evolution of chemically
776 contrasted coeval magmas: example of the Tichka plutonic complex (Morocco).
777 *Contributions to Mineralogy and Petrology* 116, 316-326.
- 778 Franceschelli, M., Puxeddu, M., Cruciani, G., Dini, A., Loi, M., 2005. Layered amphibolite
779 sequence in NE Sardinia, Italy : remnant of a pre-Variscan mafic silicic layered
780 intrusion ? *Contributions to Mineralogy and Petrology* 149, 164-180.
- 781 Graviou, P, Auvray, B., 1985. Caractérisation pétrographique et géochimique des granitoïdes
782 cadomiens du domaine nord-armoricain: implications géodynamiques. *Comptes Rendus
783 de l'Académie des Sciences de Paris* 301, 315-318.
- 784 Hallot, E., Davy P., Bremond d'Ars J. de, Auvray, B., Martin H., Van Damme H., 1996. Non-
785 newtonian effects during injection in partially crystallized magmas. *Journal of
786 Volcanology and Geothermal Research* 71, 31-44.

787 Hellström, F.A., Johansson, A., Larson, S.A., 2004. Age and emplacement of late
788 Sveconorwegian monzogabbroic dykes, SW Sweden. *Precambrian Research* 128, 39-55.

789 Johnson, M.C., Rutherford, M.J., 1989. Experimental calibration of the aluminium-in-
790 hornblende geobarometer with application to Long Valley caldera (California) volcanic
791 rocks. *Geology* 17, 837-841.

792 La Roche, H. de, Leterrier, J., Grandeclaude, P., Marchal, M., 1980. A classification of
793 volcanic and plutonic rocks using R1R2-diagrams and major-element analyses – its
794 relationships with current nomenclature. *Chemical Geology* 29, 183-210.

795 López-Moro, F.J., López-Plaza, M., 2004. Monzonitic series from the Variscan Tormes Dome
796 (Central Iberian Zone): petrogenetic evolution from monzogabbro to granite magmas.
797 *Lithos* 72, 19-44.

798 McBirney, A.R., Noyes, R.M., 1979. Crystallization and layering of the Skaergaard intrusion.
799 *Journal of Petrology* 20, 487-554.

800 McEllen, A.T., 2006. Pegmatites of the Mount Sheridan gabbro, Wichita Mountains,
801 Oklahoma. *Geological Society of America Abstracts with Programs* 38 (1), 5.

802 Momme, P., Wilson, J.R., 2002. The Kraemer Island macrodyke, East Greenland:
803 solidification of a flood basalt conduit. *Geological Magazine* 139, 171-190.

804 Paterson, S.R., 2009. Magmatic tubes, pipes, troughs, diapirs, and plumes: Late-stage
805 convective instabilities resulting in compositional diversity and permeable networks in
806 crystal-rich magmas of the Tuolumne batholith, Sierra Nevada, California. *Geosphere* 5,
807 496-527.

808 Petford, N., 2009. Which effective viscosity? *Mineralogical Magazine* 73, 167-191.

809 Peucat, J.J., Ménot, R.-P., Monnier, O., Fanning, C.M., 1999. The Terre Adélie basement in
810 the East-Antarctica shield: geological and isotopic evidence for a major 1.7 Ga thermal

811 event; comparison with the Gawler Craton in South Australia. *Precambrian Research* 94,
812 205-224.

813 Philpotts, A.R., Carroll, M., Hill, J.M., 1996. Crystal-mush compaction and the origin of
814 pegmatitic segregation sheets in a thick flood-basalt flow in the Mesozoic Hartford
815 Basin, Connecticut. *Journal of Petrology* 37, 811-836.

816 Pons, J., Barbey, P., Nachit, H., Burg, J.-P., 2006. Development of igneous layering during
817 growth of pluton: The Tarçouate Laccolith (Morocco). *Tectonophysics* 413, 271-286.

818 Roach, R.A., 1971. The layered structure of the St Peter Port Gabbro, Guernsey, Channel
819 Isles (abstract). *Journal of the Geological Society of London* 127, 295.

820 Samson, S.D., D'Lemos, R.S., 1998. U-Pb geochronology and Sm-Nd isotopic composition
821 of Proterozoic gneisses, Channel Islands, UK. *Journal of the Geological Society of*
822 *London* 155, 609-618.

823 Samson, S.D., D'Lemos, R.S., 1999. A precise late Neoproterozoic U-Pb zircon age for the
824 syntectonic Perelle quartz diorite, Guernsey, Channel Islands, UK. *Journal of the*
825 *Geological Society of London* 156, 47-54.

826 Schmidt, M.W., 1992. Amphibole composition in tonalite as a fonction of pressure: an
827 experimental calibration of the Al-in-hornblende barometer. *Contributions to*
828 *Mineralogy and Petrology* 110, 304-310.

829 Sparks, R.S.J., Huppert, H.E., 1984. Density changes during fractional crystallization of
830 basaltic magmas: fluid dynamic implications. *Contributions to Mineralogy and*
831 *Petrology* 85, 300-309.

832 Sparks, R.S.J., Huppert, H.E., Koyaguchi, T., Halloworth, M.A., 1993. Origin of modal and
833 rhythmic igneous layering by sedimentation in a convecting magma chamber. *Nature*
834 361, 246-249.

- 835 Sparks, R.S.J., Marshall, L.A., 1986. Thermal and mechanical constraints on mixing between
836 mafic and silicic magmas. *Journal of Volcanology and Geothermal Research* 29, 99-124.
- 837 Sparks, R.S.J., Meyer, P., Sigurdsson, H., 1980. Density variation amongst Mid-Ocean Ridge
838 Basalts: implication for magma mixing and the scarcity of primitive lavas. *Earth and*
839 *Planetary Science Letters* 46, 419-430.
- 840 Stewart, B.W., De Paolo, D.J., 1992. Diffusive isotopic contamination of mafic magma by
841 coexisting silicic liquid in the Muskox intrusion. *Science* 255, 708-711.
- 842 Sun, S.S., McDonough, W.F., 1989. Chemical and isotopic systematics of oceanic basalts:
843 implication for mantle composition and processes. In: Saender, A.D., Norry, M.J. (Eds),
844 *Geological Society Special Publication. Magmatism in the Ocean Basins*, vol. 42.
845 Blackwell, London, p. 313-345.
- 846 Topley, C.G., Brown, M., D'Lemos, R.S., Power, G.M., Roach, R.A., 1990. The northern
847 igneous complex of Guernsey, Channel Islands. R.S. D'Lemos, R.A. Strachan and C.G.
848 Topley (Editors), *The Cadomian Orogeny. Geological Society Special Publication* 51,
849 245-259.
- 850 Topley, C.G., Brown, M., Power, G.M., 1982. Interpretation of field relationships of diorites
851 and associated rocks with particular reference to northwest Guernsey, Channel Islands.
852 *Geological Journal* 17, 323-343.
- 853 Waight, T.E., Wiebe, R.A., Krogstad, E.J., 2007. Isotopic evidence for multiple contributions
854 to felsic magma chambers: Gouldsboro Granite, Coastal Maine. *Lithos* 93, 234-247.
- 855 Wiebe, R.A., 1974. Coexisting intermediate and basic magmas, Ingonish, Cape Breton Island.
856 *Journal of Geology* 82, 74-87.
- 857 Wiebe, R.A., 1993a. Basaltic injections into floored silicic magma chambers. *Eos*,
858 *Transactions, American Geophysical Union* 74, 1, 3.

- 859 Wiebe, R.A., 1993b. The Pleasant Bay layered gabbro-diorite, Coastal Maine: Ponding and
860 crystallization of basaltic injections into a silicic magma chamber. *Journal of Petrology*
861 34, 461-489.
- 862 Wiebe, R.A., 1994. Silicic magma chambers as traps for basaltic magmas: The Cadillac
863 Mountain intrusive complex, Mount Desert Island, Maine. *Journal of Geology* 102, 423-
864 437.
- 865 Wiebe, R.A., 1996. Mafic-silicic layered intrusions: the role of basaltic injections on
866 magmatic processes and the evolution of silicic magma chambers. *Transactions of the*
867 *Royal Society of Edinburgh: Earth Sciences* 87, 233-242.
- 868 Wiebe, R.A., Collins, W.J., 1998. Depositional features and stratigraphic sections in granitic
869 plutons: implications for the emplacement and crystallization of granitic magma. *Journal*
870 *of Structural Geology* 20, 1273-1289.
- 871 Wiebe, R.A., Frey, H., Hawkins, D.P., 2001. Basaltic pillow mounds in the Vinalhaven
872 intrusion, Maine. *Journal of Volcanology and Geothermal Research* 107, 171-184.
- 873 Wiebe, R.A., Smith, D., Sturm, M., King, E.M., Seckler, M.S., 1997. Enclaves in the Cadillac
874 Mountain Granite (Coastal Maine): Samples of hybrid magma from the base of the
875 chamber. *Journal of Petrology* 38, 393-423.
- 876 Wiebe, R.A., Wark, D.A., Hawkins, D.P., 2007. Insights from quartz cathodoluminescence
877 zoning into crystallization of the Vinalhaven granite, coastal Maine. *Contributions to*
878 *Mineralogy and Petrology* 154, 439-453.

879

880 **Figure captions**

881

- 882 Fig. 1. Geological sketch maps, location of detailed maps (including those of Fig. 2) and of
883 samples. a. North Armorican domains. b. Saint-Jean-du-Doigt intrusive complex (SJIC), from

884 Chantraine et al. (1986). Ages from Barboni et al. (2010). c. North-Guernsey intrusive
885 complex (NGIC), contours and ages from Bremond d'Ars et al. (1992) and Samson and
886 D'Lemos (1998, 1999).

887

888 Fig. 2. Geological sketch map of noteworthy outcrops and sample location. a. Poul Rodou, b.
889 Roc'h Louet, and c. Primel from the SJIC (this work). d. The Beaucette Battery, and e. The
890 Beaucette pass from the NGIC (this work and Bremond d'Ars et al., 1992).

891

892 Fig. 3. Photographs of sheets and diapirs in the SJIC sampled sections. a. Section SJ34 and
893 sample position. Hammer for scale. b. Section SJ43 and sample position. Hammer for scale.
894 c. A dioritic sheet with feeding roots, under a xenolith. d. A concave-down diapir within the
895 gabbro, just below a not visible dioritic sheet.

896

897 Fig. 4. Mixing, mingling, magmatic brecciation and pegmatoid in the SJIC (Saint-Jean's bay).
898 a. Gabbroic pillow-like enclave with a chilled margin, enclosed in a heterogeneous
899 monzogabbro (mingling). b. Ribbon rocks in the process of hybridization (mingling/mixing).
900 Hammer for scale. c. Jigsaw-type breccias with polyhedral mafic enclaves enclosed in a
901 texturally homogeneous (intergranular) monzonite forming a vein network. A few blocky
902 clasts present mixing/mingling evidence (not visible). d. Mafic cumulate-aplite-pegmatoid
903 association. Sample PM2 (three analyses in Table 1).

904

905 Fig. 5. Sheets and diapirs in the NGIC. a. Photograph of section GS10 and sample position.
906 Hammer for scale. b. Detail: gabbroic sheet and inclined pipes. Pencil for scale. c.
907 Photograph of section GS13 and sample position. d. Sketch of the dioritic veins. e. Sketch of
908 the inclined pipes. f. Cross-section through a zoned pipe, with a core (dark gray) less

909 differentiated than the rim (light gray), a pegmatitic upper part (white), and altered overlying
910 host rock. d, e and f from Elwell et al. (1960).

911

912 Fig. 6. Cumulates and pegmatoids from the NGIC (Spur Point, Saint Peter Port gabbro). a.
913 Mottled orthocumulate showing layers of poikilitic amphibole crystal flecks. Pencil for scale.
914 b. Photomicrograph (crossed nicols) of the Spur Point mottled orthocumulate (sample GS1a,
915 fleck-free white layer). Cumulus minerals are calcic plagioclase (Pl), hornblende (Hb) and
916 clinopyroxene (Cpx). By decreasing abundance, intercumulus phases are plagioclase,
917 clinopyroxene, orthopyroxene, Fe-Ti oxides, and apatite. c. Mafic cumulate-pegmatoid
918 association.

919

920 Fig. 7. NGIC plagioclase compositions. a. Anorthite content in plagioclases of samples GS1a
921 (26 analyses), GS7d, e, l (21 analyses), and GS13a (16 analyses). b. Anorthite profile through
922 a plagioclase from GS13a.

923

924 Fig. 8. Chemical sections in the SJIC. MgO, TiO₂ and Al₂O₃ concentrations through sections
925 SJ34 and SJ43 (located in Fig. 2a and shown in Fig. 3a and b). Microtextural sketches, shown
926 for samples SJ34a, d2, and e, evidence the lack of chilled margins (white: plagioclase; grey:
927 amphibole and altered olivine; black: Fe-Ti oxides).

928

929 Fig. 9. Chemical sections in the NGIC. MgO, TiO₂ and Al₂O₃ contents through sections
930 GS10-13 and GS7 (located in Fig. 2d and e).

931

932 Fig. 10. Magmatic affinities of the mafic rocks from the SJIC and NGIC. Position of the
933 gabbroic samples in the diagram La/10-Y/15-Nb/8 (Cabanis and Lecolle, 1989).

934

935 Fig. 11. Chondrite C1-normalized rare earth elements (REE) patterns of representative SJIC
936 and NGIC samples. Normalization values from Sun and McDonough (1989). a. Sheet-diapir
937 pairs SJ34 and SJ43, together with the corresponding gabbroic field (SJIC). b. Selected SJIC
938 samples. c. Macrorhythms, sheets and a pipe from the NGIC. d. Granite, sheet and cumulate
939 from the NGIC.

940

941 Fig. 12. Models of replenishment and crystallization. Time proceeds along the “*t*-box” line.
942 a. b. c. Model for Poul Rodou in the SJIC. A gabbroic (θ) reservoir crystallizes from below:
943 crystal settling is negligible so that the resulting gabbro is almost homogeneous. A dioritic
944 magma (δ) with about $\chi=30\%$ phenocrysts enters the crystallizing gabbro. First buoyant at the
945 base, while rising it crosses levels of neutral buoyancy (assuming negligible crystal
946 resorption) where it spreads to form sheets from which diapirs are then extracted. ρ is density
947 at given temperature (calculated from Bottinga and Weill, 1970) and crystal content (χ for δ ;
948 grey scale to the right for θ ; see text). Insets are detailed zones of a and b.
949 d. e. f. g. h. i. Model for Beaucette in the NGIC. Mafic recharges (d, g) and crystal settling,
950 first of mafic minerals alone (e), second of mafic crystals and plagioclase (f) account for the
951 layering and the heterogeneities of the gabbros. Then late dioritic recharges (h) and
952 subsequent evolution (i, see text) explain most of the observed features.

953

954 Fig. 13. A comprehensive model for the SJIC reservoir. The straight line locates the observed
955 Poul Rodou/Saint-Jean’s bay/Primel coastal cross-section. See text for explanations.

Table 1. Chemical data (wt% oxide, ppm element) on whole rock samples from Saint-Jean-du-Doigt and North-Guernsey.

Location	R. Louet	P. Rodou	Primel	St-J. W	St-J.W	St-J.E	P. Rodou	P. Rodou	P. Rodou	P. Rodou	P. Rodou	P. Rodou	P. Rodou	P. Rodou	P. Rodou
Sample	SJ32	SJ44b	SJ16	SJ17	SJ19	SJ17	SJ22	SJ34a	SJ34c	SJ34b1	SJ43a	SJ43c	SJ43d		
Texture	Cum.	Gr./Cum	Peg.	Gr.	Gr.	Gr.	Gr.	Gr.	Gr.	Gr./Cum.	Gr.	Gr.	Gr./Peg.		
Emplacement	Cum.	Intrusion	Intrusion	Ang. Cl	Intrusion	Ang. Cl	Intrusion	Intrusion	Sheet	Diapir	Intrusion	Sheet*	Diapir		
Type	Melagab.	Melagab.	Gabbro	Q-Monz.	Gabbro	Q-Monz.	Granite	Gabbro	Diorite	Diorite	Gabbro	Q-Monz.	Q-Monz.		
SiO ₂	(wt.%) 44.20	47.10	49.20	50.20	53.25	58.60	76.75	49.70	60.80	58.80	50.00	72.20	74.00		
TiO ₂	0.80	0.64	1.92	2.22	2.42	1.37	0.13	1.81	1.24	0.65	1.79	0.33	0.13		
Al ₂ O ₃	14.32	14.22	15.40	14.53	14.80	17.75	12.05	15.00	15.55	16.90	15.42	14.05	10.62		
Fe ₂ O ₃ ^t	12.80	9.40	9.80	9.96	11.58	7.00	1.62	10.90	5.58	5.80	11.25	1.98	4.32		
MnO	0.21	0.15	0.14	0.19	0.20	0.10	0.02	0.19	0.10	0.09	0.18	0.03	0.03		
MgO	13.00	13.90	6.85	6.92	3.69	1.92	0.10	6.80	2.47	1.18	7.23	0.78	0.19		
CaO	10.30	8.50	11.47	12.15	7.20	5.00	0.24	9.40	8.40	14.60	7.38	2.14	8.70		
Na ₂ O	0.88	1.52	2.85	2.69	3.67	5.55	3.38	2.86	4.50	0.23	2.48	6.85	0.29		
K ₂ O	0.26	0.85	0.48	0.22	1.46	1.49	4.70	1.13	0.37	0.23	2.30	0.36	0.24		
P ₂ O ₅	0.03	0.14	0.14	0.30	0.72	0.32	0.02	0.23	0.26	0.19	0.25	0.05	0.02		
L.O.I.	3.48	3.41	1.27	0.61	0.64	0.81	0.56	1.83	1.02	1.60	2.08	0.58	1.02		
Total	100.07	99.83	99.52	99.99	99.63	99.91	99.57	99.85	100.29	100.27	100.36	99.35	99.56		
Rb	(ppm) 7.5	27.4	17.3	6.4	42.4	42.5	185	37.5	9.4	7.9	111	8.6	15.5		
Sr	142	253	239	145	218	235	23	233	322	695	121	84	445		
Ba	50	123	91	19	405	405	324	286	90	49	330	35	32		
Sc	29.0	29.5	47	45	28.0	8.7	2.5	40	17	6.5	38	5.2	1.2		
V	143	210	405	347	265	145	4	290	147	90	281	52	32		
Cr	216	955	38	103	35	9	3.5	255	25	13	225	11	5		
Co	70	57	38	47	25	15	2	39	11	5	41	5	2		
Ni	213	380	44	55	19	9	2	70	17	12	72	7	4		
Y	9.6	5.6	23.5	38.0	65	38.8	54	32.5	47.0	33.0	30.5	21.8	9.3		
Nb	2.8	2.5	7.9	14.3	37.5	25.0	30.0	16.0	30.5	21.5	14.0	15.4	5.2		
La	2.5	7.1	6.4	10.8	35.0	29.5	30.0	11.0	20.5	27.0	11.0	10.0	24.5		
Ce	5.3	16.0	14.5	25.0	80	60	86	25.0	45	56	24.0	16.5	38.0		
Nd	3.4	10.0	11.2	17.8	45.0	30.5	28.5	17.0	26.6	27.0	16.0	8.0	11.0		
Sm	1.35	2.70	2.95	5.1	10.4	6.4	6.6	4.7	6.4	5.5	4.5	2.25	1.75		
Eu	0.61	0.84	1.10	1.78	2.67	2.62	0.60	1.56	1.68	1.89	1.44	1.08	1.11		
Gd	1.2	2.7	4.1	6.5	11.0	7.2	6.9	5.7	7.6	5.8	5.2	2.9	2.1		
Dy	1.55	2.45	4.1	6.5	10.9	6.4	8.2	5.5	7.8	5.4	5.4	3.15	1.4		
Er	0.9	1.5	2.2	3.7	6.1	3.7	5.5	3.1	4.6	3.3	3.1	2.2	1.0		
Yb	0.90	1.48	2.10	3.42	5.60	3.62	6.52	2.92	4.46	3.36	2.90	2.20	1.01		
Th	0.30	1.15	1.25	0.55	3.50	5.05	17.3	1.40	6.15	12.3	1.20	13.7	4.50		

ICP-AES analyses (analyst: Jo Cotten, Brest). Cum.: Cumulat; Gr.: Granular (broad sense); Peg.: pegmatitic; Dol.: Doleritic; Apl.: Aplitic; Fl. cl.: Fluidal clast; Ang. cl.: Angular clast; Sheet*: upper part of a sheet; L.O.I.: Loss on ignition.

Table 1 (continuation).

Location	Primel PM2a	Primel PM2b	Primel PM2c	Spur GS1a	Cobo GS8	Beaucette GS10d	Beaucette GS10f	Beaucette GS13a	Beaucette GS10c	Beaucette GS7a	Beaucette GS7e	Beaucette GS7j	Beaucette GS7c
Sample	Peg.	Apl.	Cum.	Cum.	Gr.	Gr./Cum.	Gr./Cum.	Gr.	Gr.	Gr./Cum.	Gr./Cum.	Gr./Cum.	Gr.
Texture	Intrusion	Intrusion	Intrusion	Intrusion	Intrusion	Macrorh.	Macrorh.	Sheet	Diapir	Macrorh	Macrorh	Macrorh	Sheet
Emplacement	Gabbro	Gabbro	Gabbro	Gabbro	Granite	Melagab.	Melagab.	Gabbro	Mzdiior.	Melagab.	Gabbro	Gabbro	Sheet
Type	Gabbro	Gabbro	Gabbro	Gabbro	Granite	Melagab.	Melagab.	Gabbro	Mzdiior.	Melagab.	Gabbro	Gabbro	Diorite
SiO ₂	(wt%) 52.60	48.40	49.00	45.30	76.00	47.70	49.70	48.50	61.80	49.30	53.50	51.90	66.20
TiO ₂	0.59	0.57	0.39	1.16	0.10	0.57	0.82	1.09	0.06	0.63	0.82	0.74	0.13
Al ₂ O ₃	17.30	17.25	19.20	20.45	12.40	11.75	18.15	20.80	21.40	13.50	16.85	15.80	16.30
Fe ₂ O ₃ ^t	5.16	7.67	5.70	9.55	1.48	10.45	8.93	9.75	1.35	9.00	8.60	8.15	1.60
MnO	0.09	0.11	0.09	0.13	0.05	0.17	0.15	0.14	0.03	0.14	0.14	0.12	0.02
MgO	6.50	8.85	7.34	5.56	0.24	14.35	6.09	3.60	1.14	12.30	5.23	7.35	1.08
CaO	12.45	12.15	14.10	14.00	0.55	9.20	10.40	9.75	5.32	9.60	8.18	9.40	7.10
Na ₂ O	3.40	2.21	2.17	1.75	3.61	1.20	2.88	3.40	5.89	2.08	3.21	3.00	5.20
K ₂ O	0.32	0.13	0.13	0.97	3.23	0.88	0.80	1.03	1.51	0.95	1.38	1.25	0.52
P ₂ O ₅	0.10	0.04	0.03	0.21	0.04	0.09	0.14	0.27	0.05	0.08	0.14	0.12	0.17
L.O.I.	1.61	2.27	2.02	1.07	0.92	3.25	1.45	1.59	1.46	2.12	1.73	1.91	1.98
Total	100.12	99.65	100.17	100.15	98.62	99.61	99.51	99.92	100.01	99.70	99.78	99.74	100.30
Rb	(ppm) 11.5	3.3	3.7	27.2	124	26.0	20.0	29.5	42.0	28.0	40	35.0	13.2
Sr	277	217	266	872	113	172	420	590	867	340	430	340	280
Ba	54	25	22	300	656	298	226	481	351	370	310	190	88
Sc	44	44	44	38	3.3	37	34	26.0	3.9	40	31	44	5
V	184	202	154	317	8	205	253	246	12	210	242	232	28
Cr	179	232	240	72	4	855	195	18	8	1100	138	370	6
Co	25	35	25	32	2	59	31	24	5	50	30	37	7
Ni	50	72	70	24	2	242	42	9	12	265	35	86	8
Y	16.8	14.6	8.8	16.0	12.2	12.6	17.3	24.8	4.4	16.0	19	16.0	6.5
Nb	2.7	1.2	0.4	5.2	11.2	2.3	3.2	6.0	0.7	2.5	4.2	3.7	1.0
La	3.4	2.6	1.7	11.2	18.0	7.8	11.2	15.6	10.5	8.0	12.5	9.4	12.5
Ce	9.5	6.0	4.0	27.0	34.5	15.5	23.5	35	15	18.0	26.0	21.0	22.0
Nd	6.1	4.3	2.0	18.0	12.8	8.4	12.7	22.0	4.2	10.0	14.1	12.1	8.0
Sm	2.00	1.80	1.10	4.2	2.35	2.05	3.0	4.8	0.6	2.75	3.4	3.1	1.5
Eu	0.83	0.90	0.55	1.45	0.43	0.75	1.09	1.40	0.64	0.88	0.99	0.94	0.59
Gd	2.8	2.5	1.55	3.5	2.5	1.9	3.0	4.5	0.6	2.6	3.65	2.8	1.6
Dy	2.85	2.55	1.55	2.95	2.10	2.05	2.90	4.3	0.65	2.65	3.15	2.80	1.15
Er	1.6	1.5	0.8	1.5	1.3	1.3	1.7	2.4	0.5	1.6	1.9	1.6	0.6
Yb	1.50	1.31	0.78	1.30	1.49	1.18	1.67	2.28	0.56	1.62	1.83	1.58	0.57
Th	0.15	0.20	0.10	0.20	11.4	1.35	1.35	1.45	2.75	2.85	3.5	1.90	3.40

Table 2. Isotopic data on whole rock samples from Saint-Jean-du-Doigt and North-Guernsey.

Location	Type	Sample	Rb ppm	Sr ppm	$^{87}\text{Rb}/^{86}\text{Sr}$	$^{87}\text{Sr}/^{86}\text{Sr}$	$\pm 2\sigma_m$ ($\times 10^{-6}$)	$(^{87}\text{Sr}/^{86}\text{Sr})_i$	Sm ppm	Nd ppm	$^{147}\text{Sm}/^{144}\text{Nd}$	$^{143}\text{Nd}/^{144}\text{Nd}$	$\pm 2\sigma_m$ ($\times 10^{-6}$)	ϵ_{Nd}
<i>Saint-Jean-du-Doigt</i>														
Primer	Dolerite	SJ14	5.98	142	0.122	0.704655	11	0.7041	4.88	17.51	0.1684	0.512846	6	5.3
Primer	Peg.	SJ16	18.5	243	0.221	0.704947	9	0.7039	3.02	10.43	0.1750	0.512829	6	4.7
P. Rodou	Gabbro	SJ34a	38.0	230	0.477	0.707216	9	0.7049	4.22	15.88	0.1609	0.512860	4	5.9
P. Rodou	Diorite	SJ34c	8.71	296	0.085	0.707338	10	0.7069	6.28	25.38	0.1496	0.512668	7	2.6
St-J. W	Mzgab.	SJ37	42.1	208	0.586	0.707246	12	0.7043	10.04	43.62	0.1391	0.512633	7	2.4
St-J. W	Monz.	SJ9	42.3	226	0.541	0.707339	30	0.7047	6.36	30.04	0.1279	0.512632	5	2.9
St-J. E	Q-Monz.	SJ17	14.0	241	0.167	0.707263	10	0.7064	2.55	10.95	0.1407	0.512676	6	3.2
P. Rodou	Granite	SJ22	185	21.6	25.1	0.819524	15	0.6935	5.86	26.58	0.1334	0.512650	5	3.0
<i>North-Guernsey (data from Brémond d'Ars et al., 1992)</i>														
Spur	Cum.	64A (GS1a)	18.1	891	0.059	0.70627	-	0.7058	-	-	-	-	-	-
Beaucette	Melag.	27A (GS7a)	34.2	275	0.360	0.70842	-	0.7056	-	-	-	-	-	-
Beaucette	Gabbro	26B (GS10f)	41.9	379	0.321	0.70836	-	0.7058	-	-	-	-	-	-
Beaucette	G. sheet	27E (GS13a)	73.7	564	0.378	0.70867	-	0.7057	-	-	-	-	-	-
Cobo	Granite	74-71 (GS8)	127	101	3.64	0.73417	-	0.7055	-	-	-	-	-	-

See text for analytical methods and calculation of ϵ_{Nd} ; index i for initial.

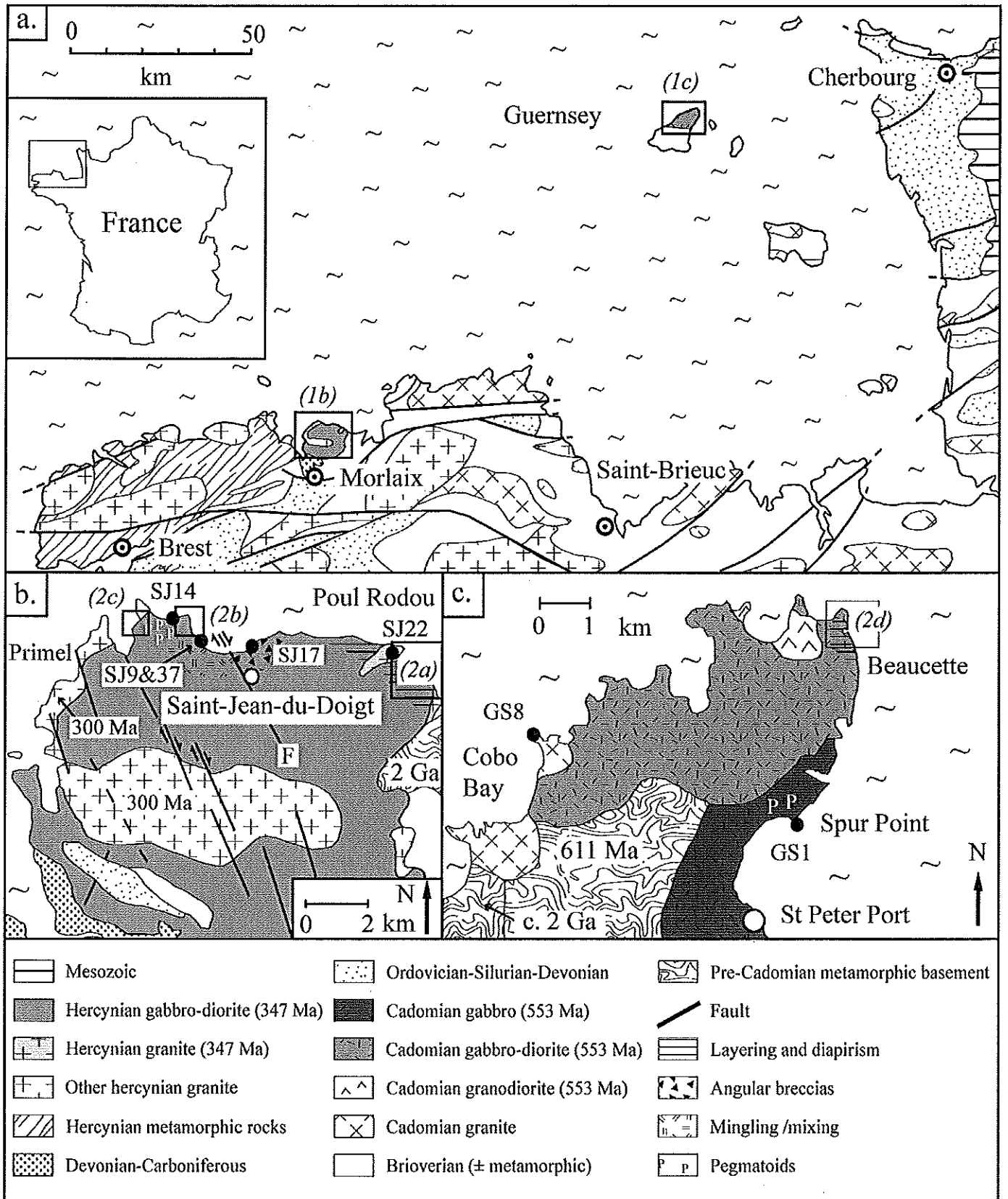


Fig. 1

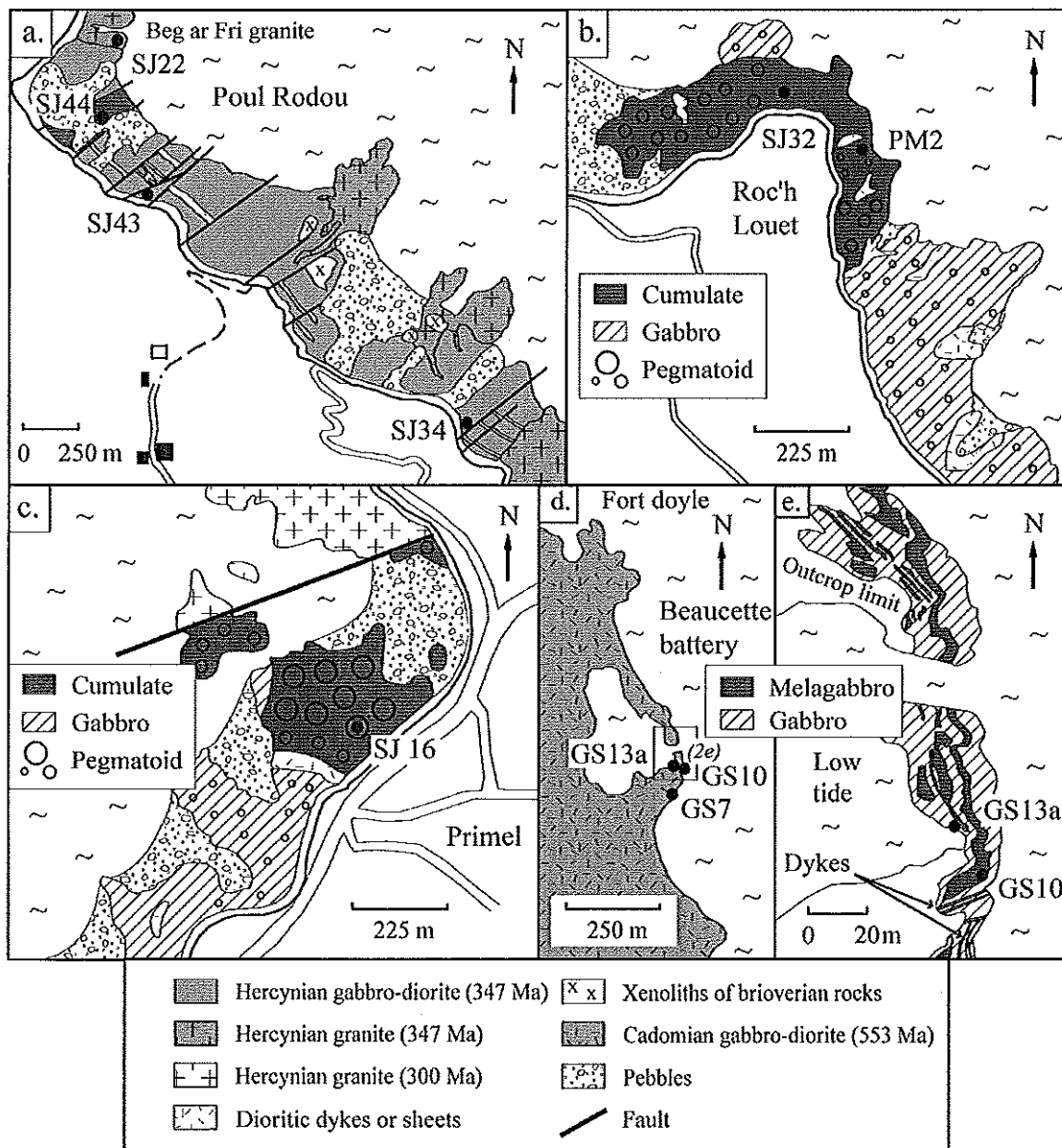


Fig. 2

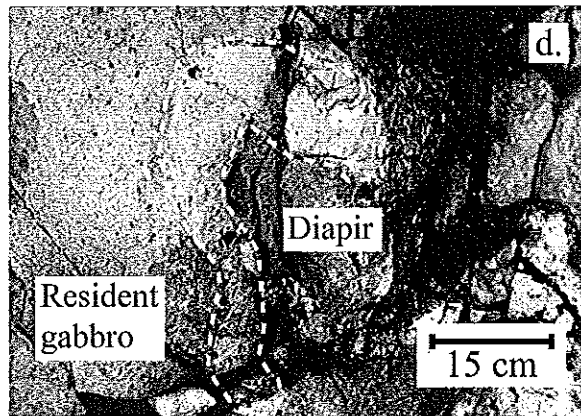
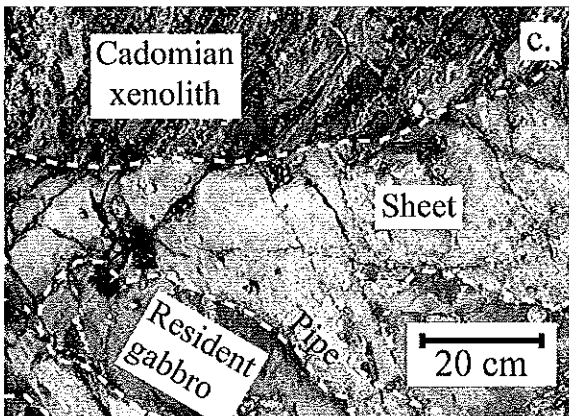
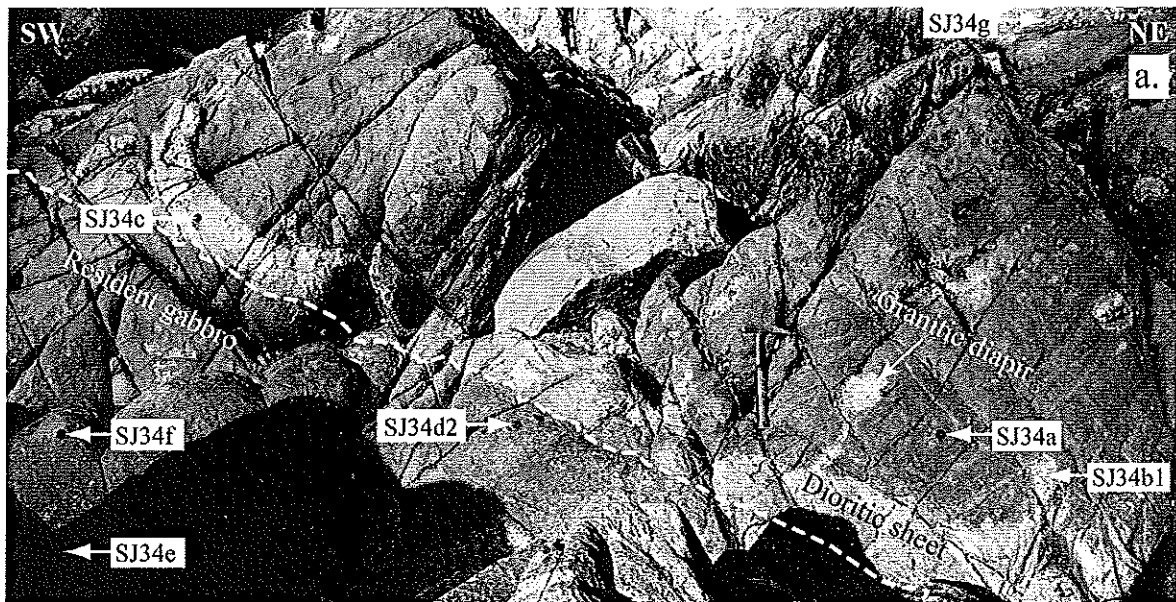


Fig. 3

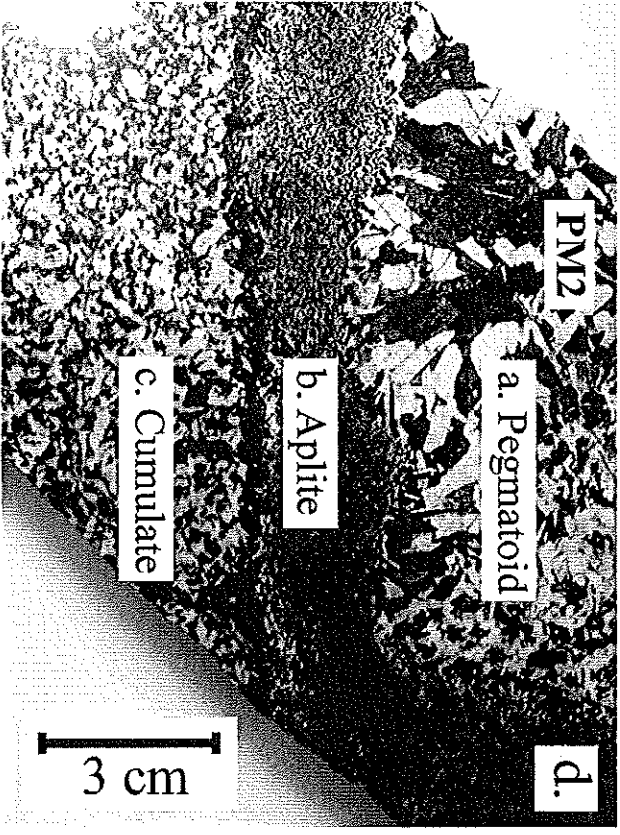
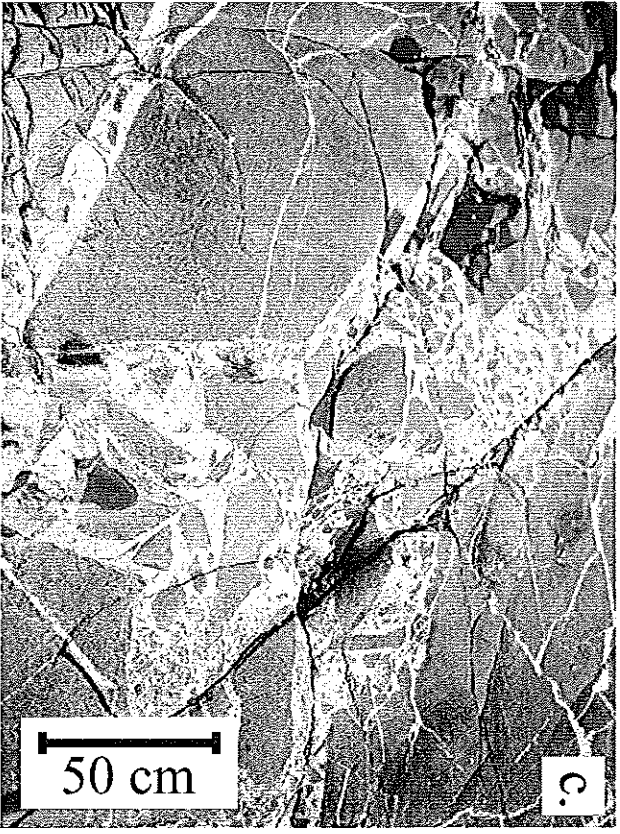
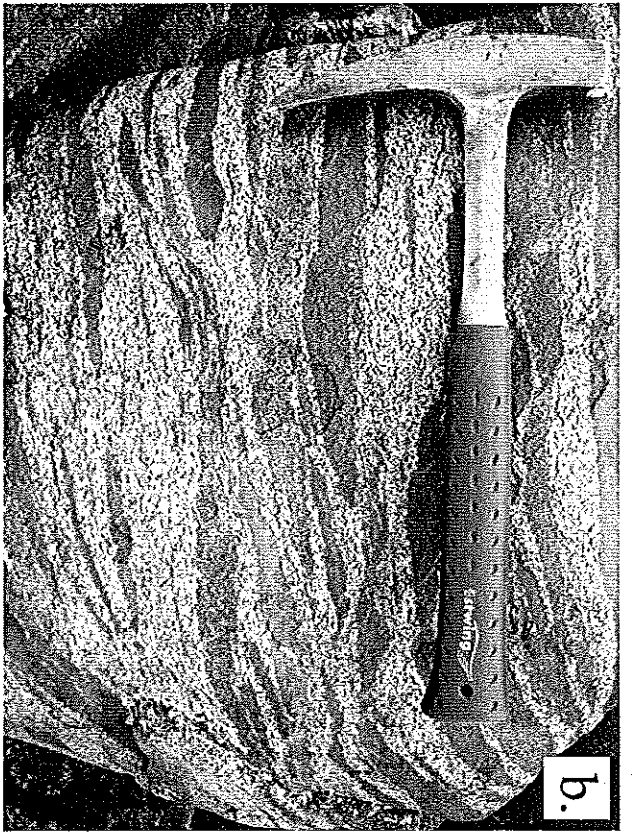
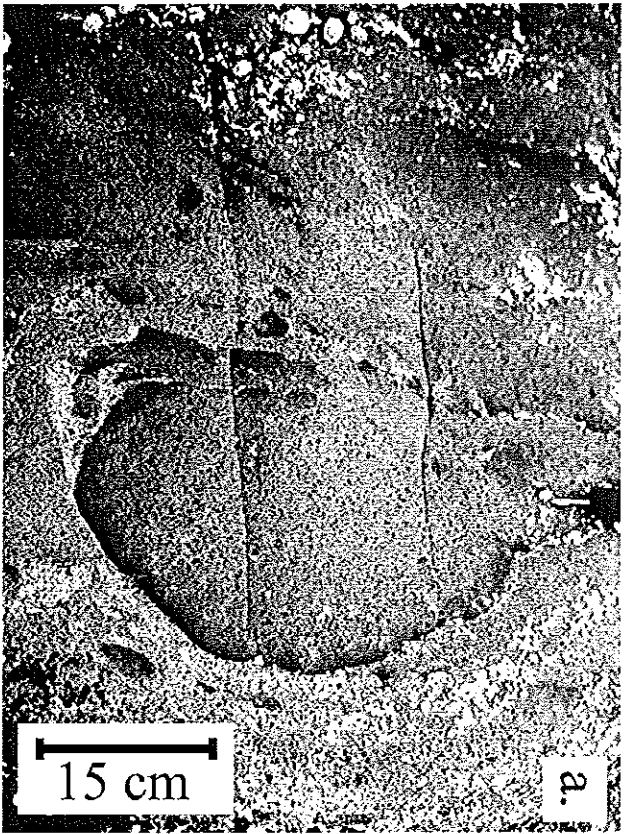


Fig. 4

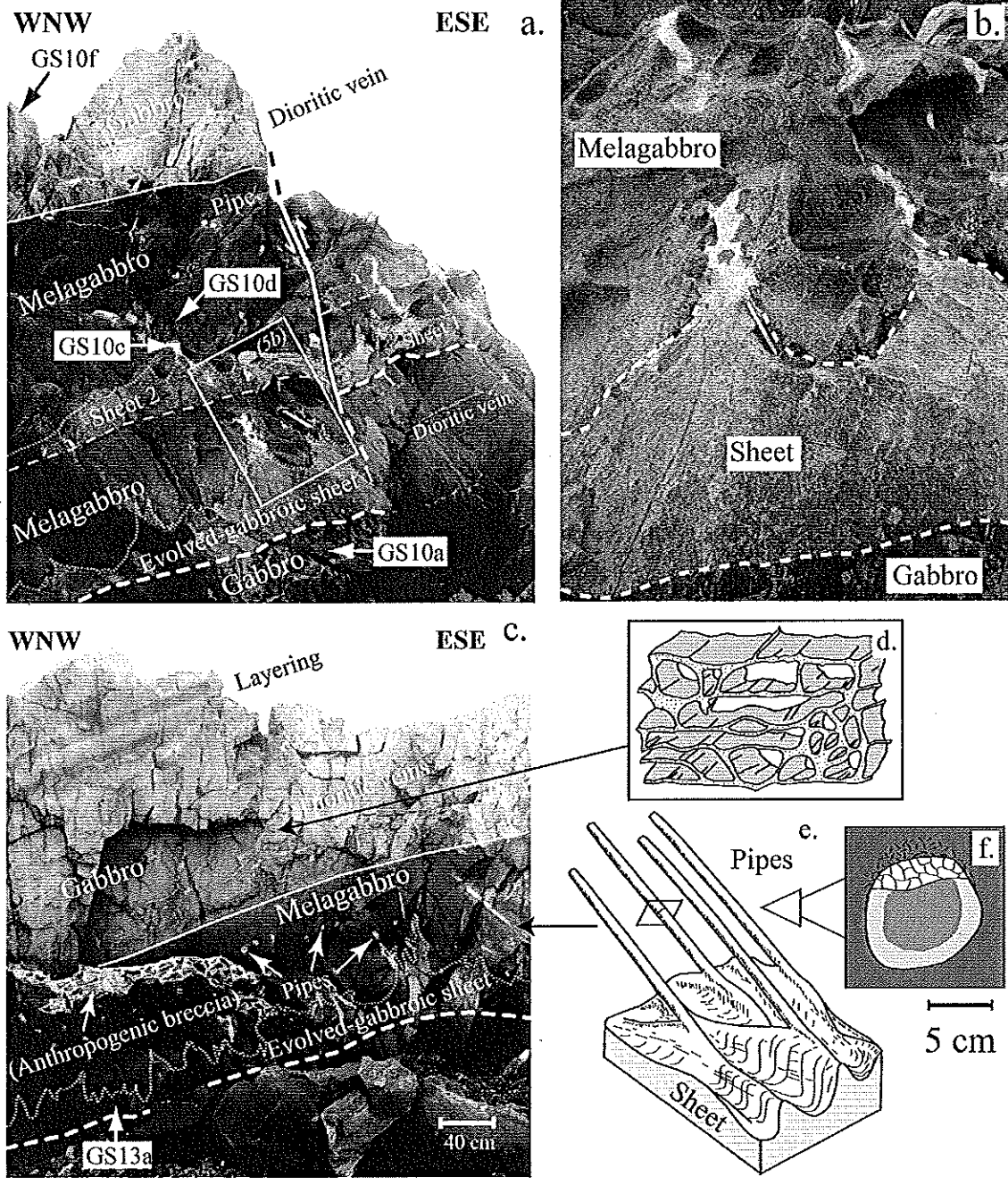


Fig. 5

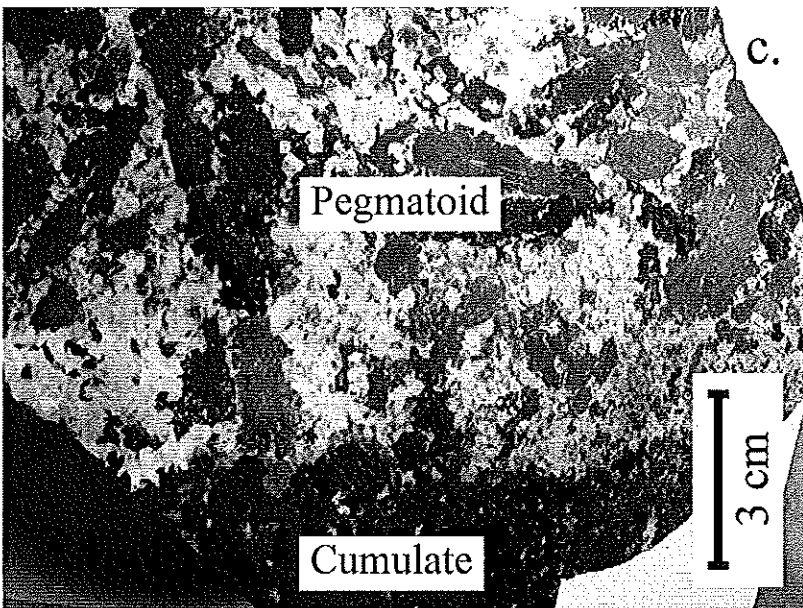
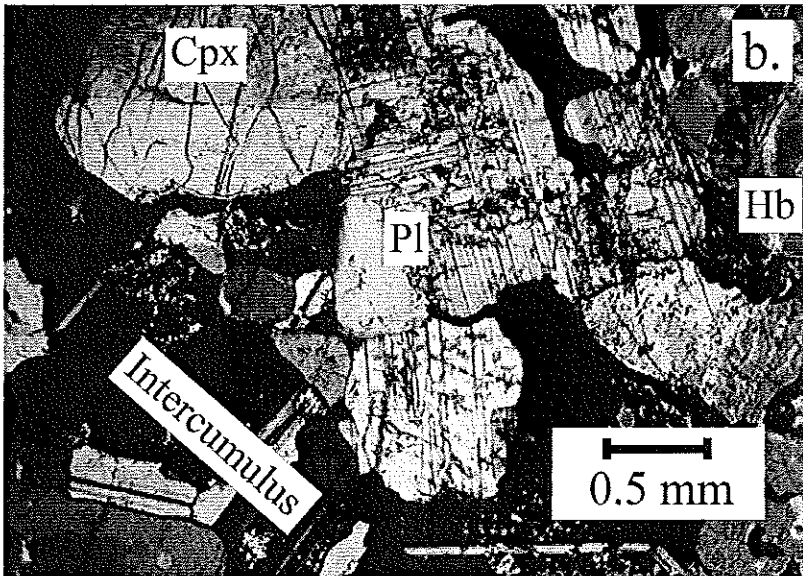


Fig. 6

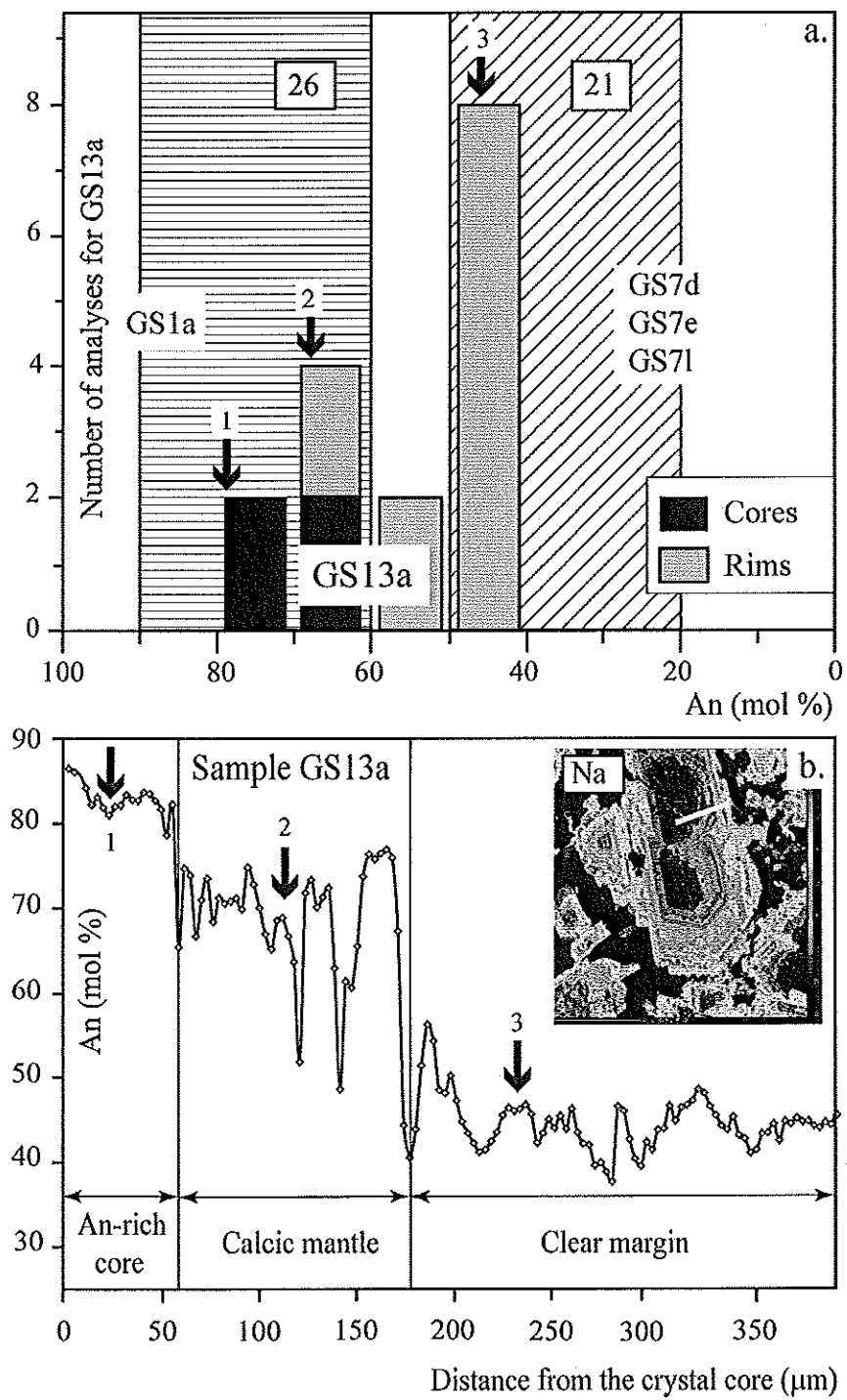


Fig. 7

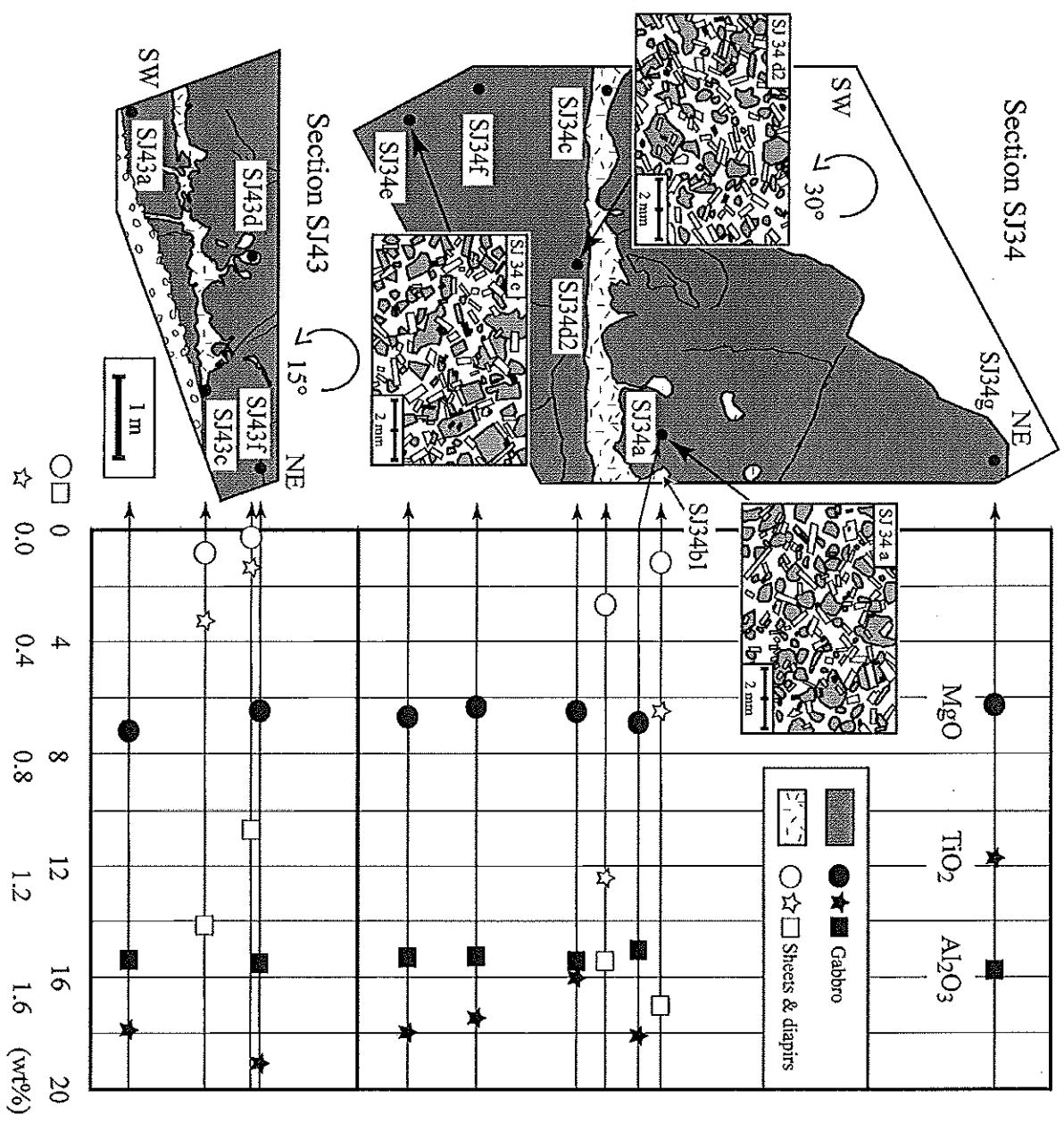


Fig. 8

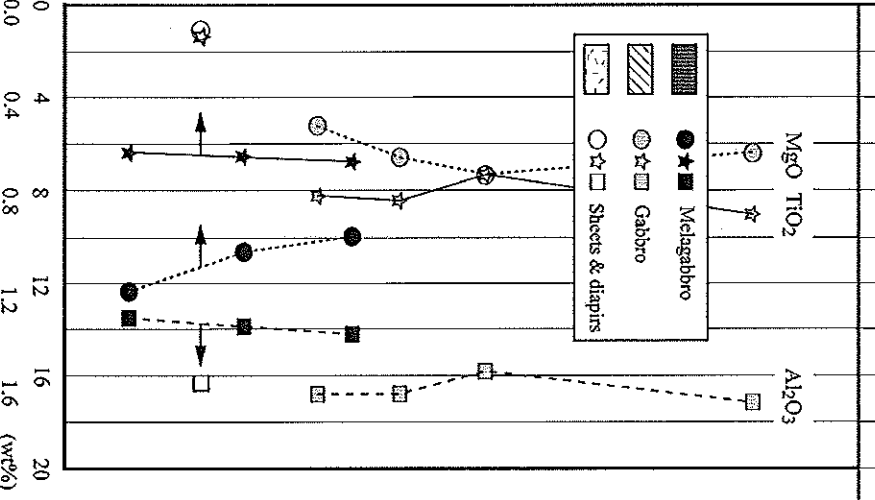
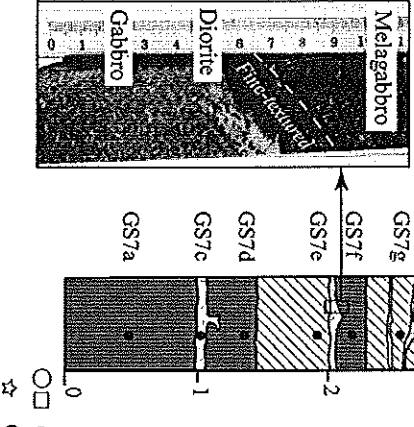
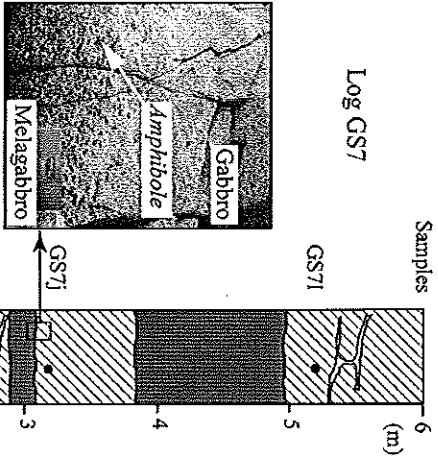
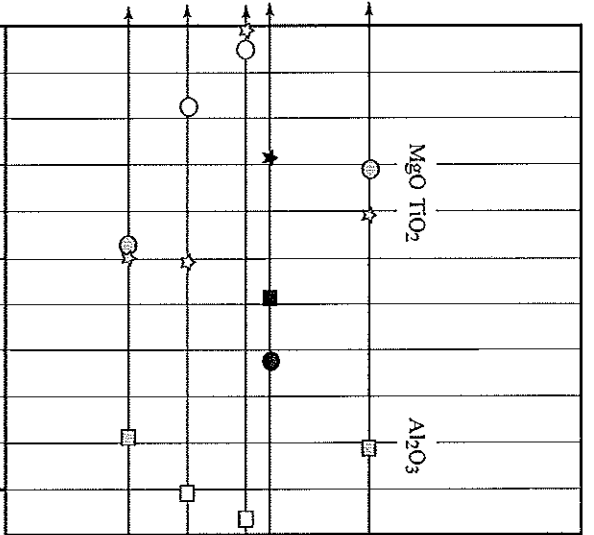
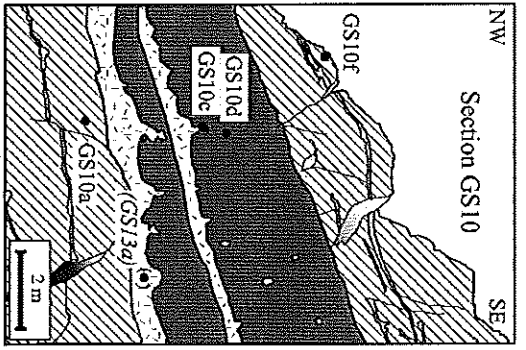


Fig. 9

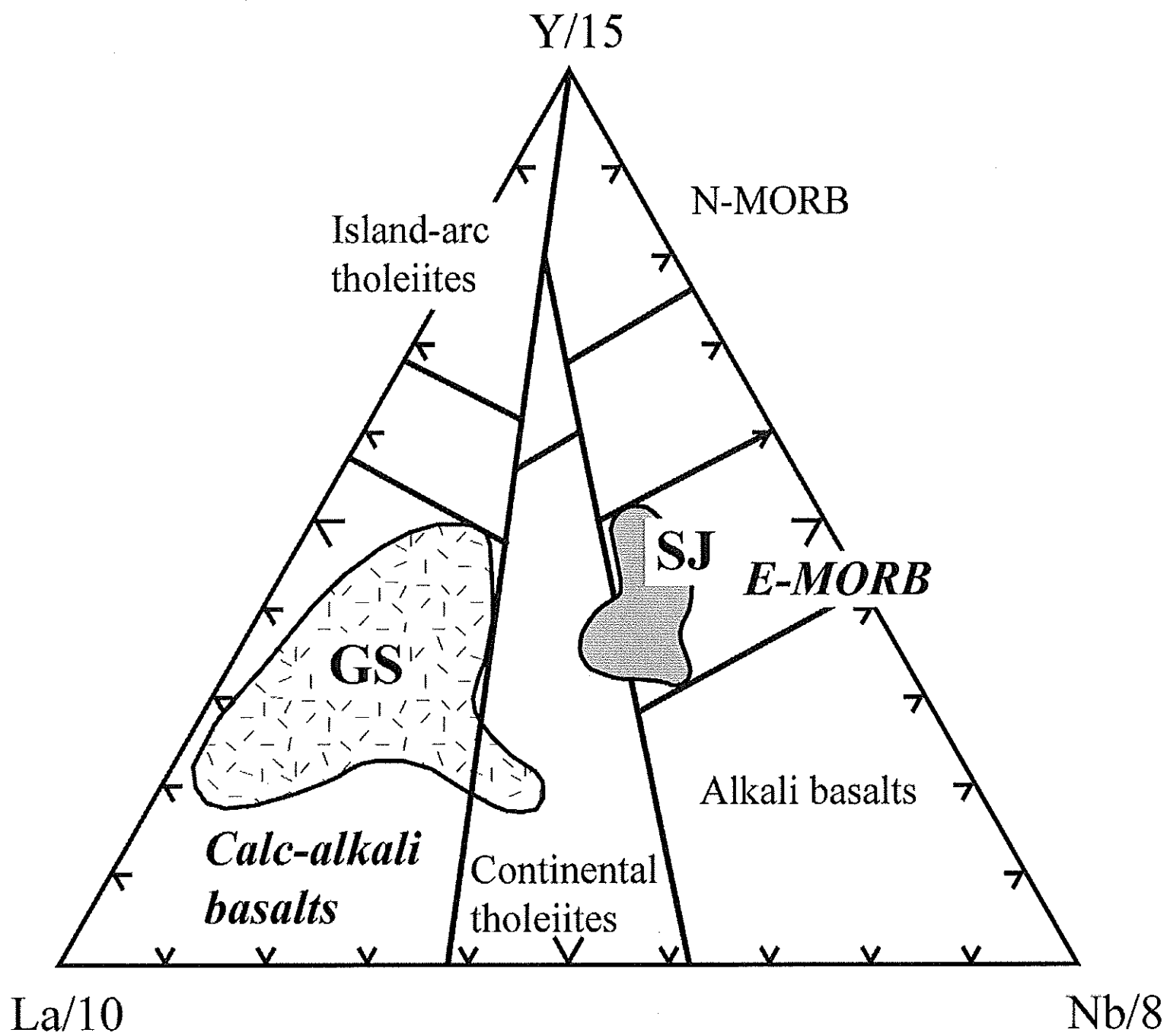


Fig. 10

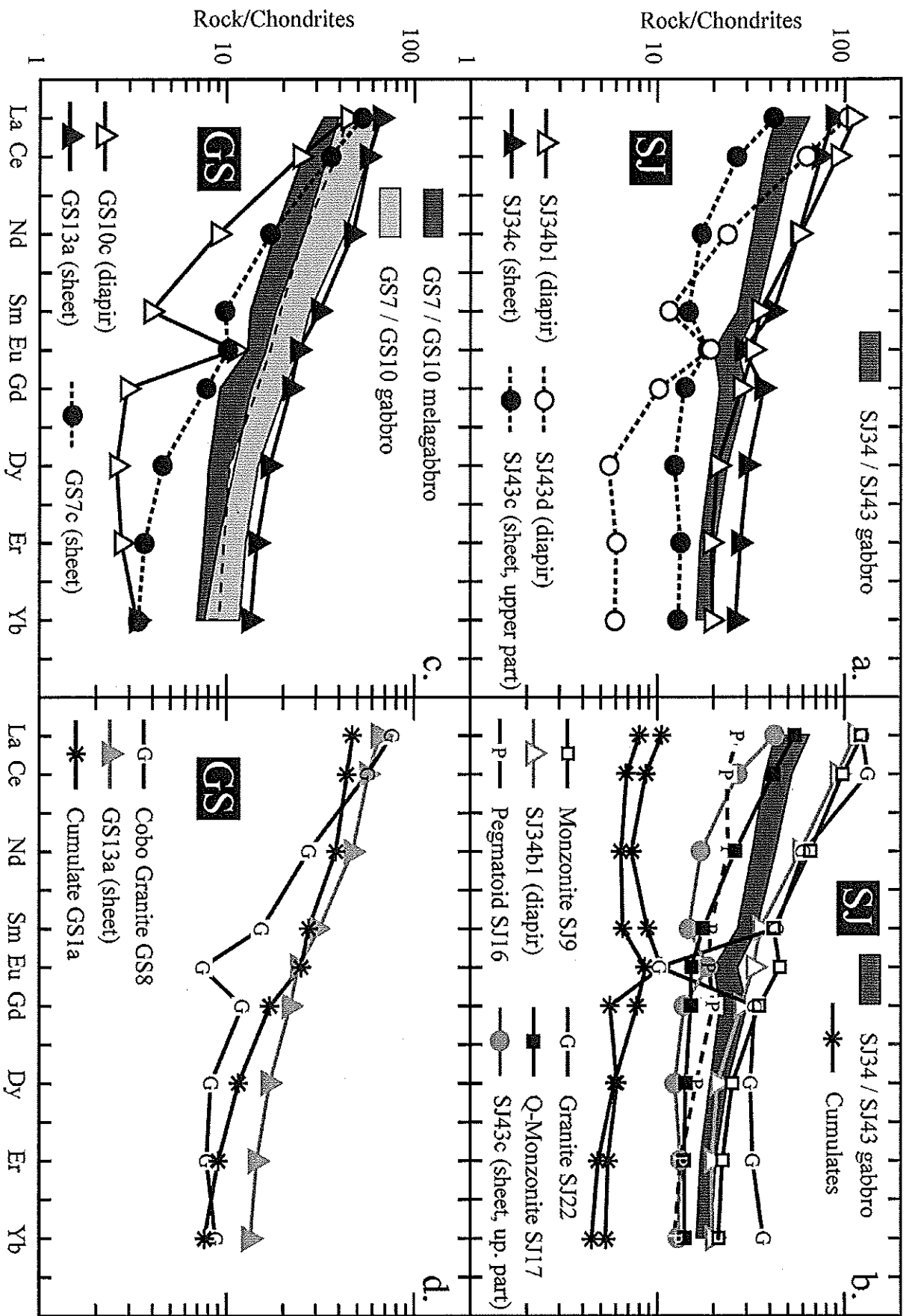


Fig. 11

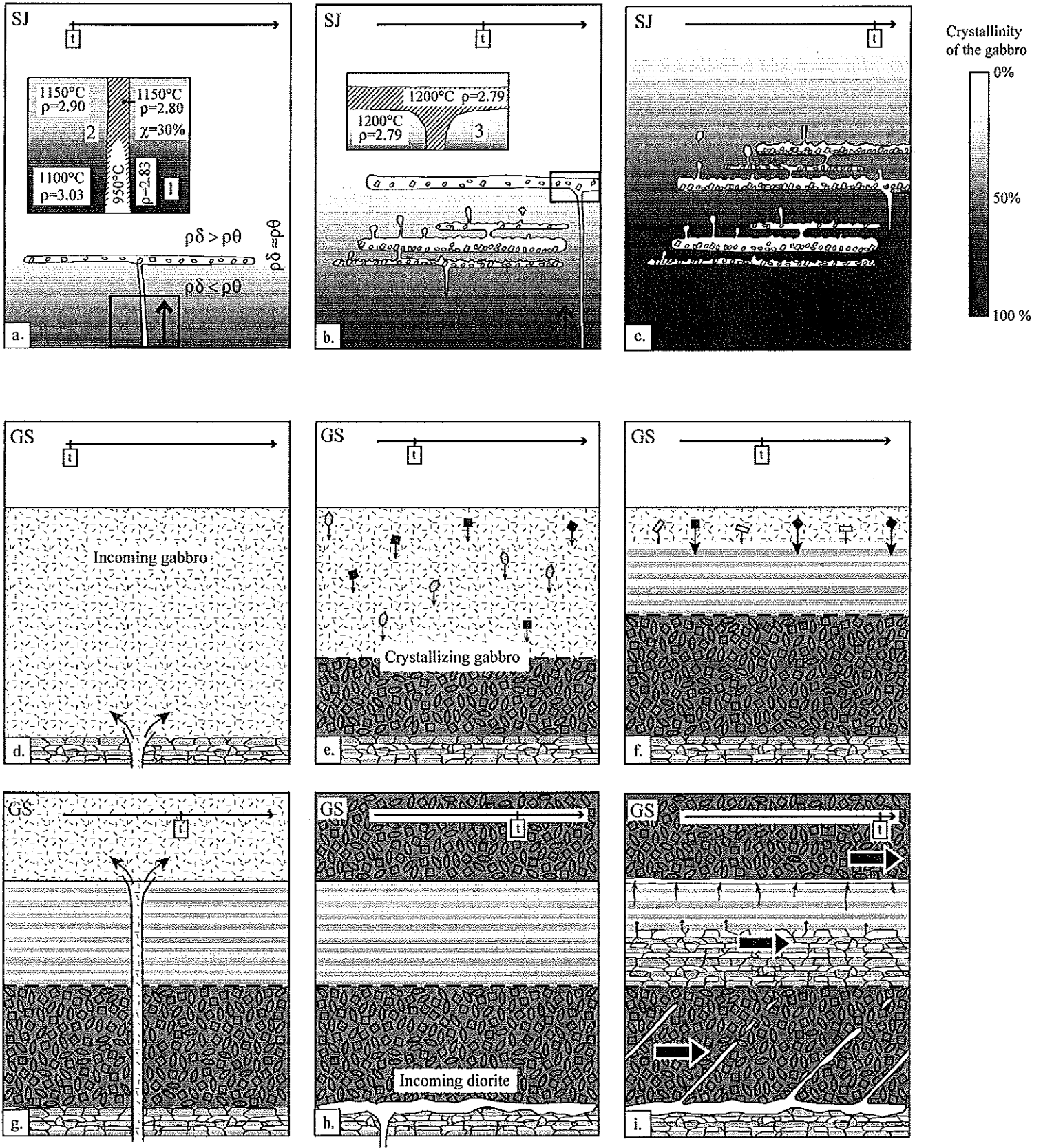
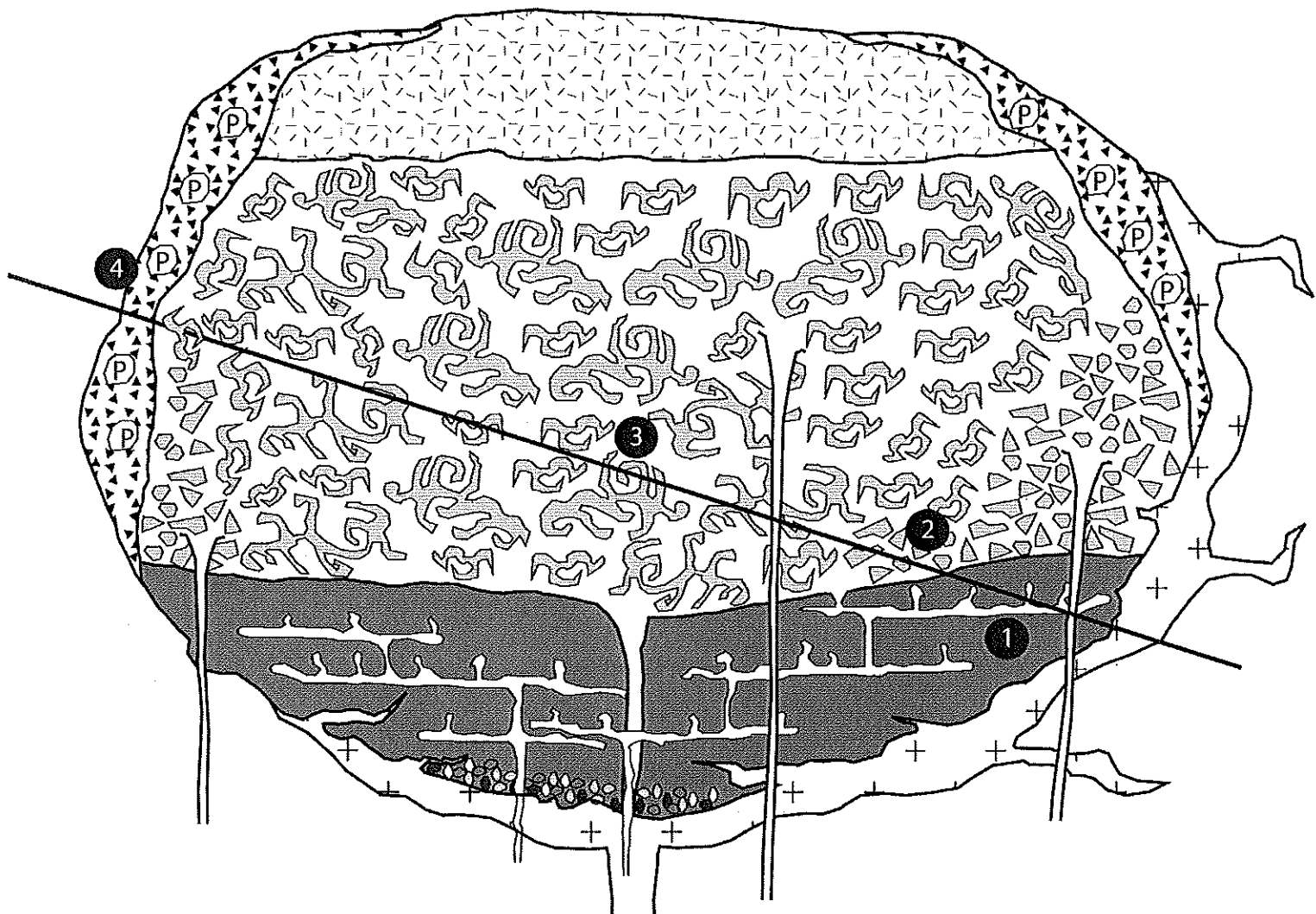


Fig. 12



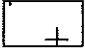
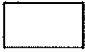
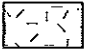








- | | | | |
|---|---------------------------|---|--|
|  | Granite |  | Diorite |
|  | Hybridized magma |  | Gabbro from Poul Rodou |
|  | Lobate facies |  | Amphibole-rich cumulate |
|  | Angular breccia |  | Cross-section from Poull Rodou (1) to Primel (4) through Saint-Jean (2, 3) |
|  | Plagioclase-rich cumulate |  | |
|  | Pegmatoid | | |

Fig. 13